DEVELOPMENT OF A RATIONAL MECHANISTIC-EMPIRICAL BASED DESIGN GUIDE FOR THIN AND ULTRA-THIN WHITETOPPING

Climatic Considerations

University of Pittsburgh
Department of Civil and Environmental Engineering
Pittsburgh, Pennsylvania 15261

Prepared by:
Manik Barman
Nicole Dufalla
Zichang Li
Feng Mu
Julie M. Vandenbossche, Ph.D., P.E.

Prepared for:
FHWA Pooled Fund Project: TPF-5-165

August 2013

CONTENTS

LIST OF FIGURES iv

1. INTRODUCTION 1

2. CHARACTERIZATION OF HMA MODULUS 4

2.1. Factors affecting the HMA Temperature 4

2.1.1. Effect of PCC Layer Thickness 7

2.1.2. Effect of HMA Layer Thickness 8

2.1.3. Effect of Seasons 8

2.1.4. Effect of Geographical Location (Climate) 9

2.2. Characterization of HMA Modulus 14

2.4. Procedure to Characterize the HMA Modulus 39

2.5. Summary of HMA Modulus Characterization 40

3. TEMPERATURE GRADIENT WITHIN THE PCC OVERLAY 40

3.1. Populating Database of Hourly Nonlinear Temperature Gradients for Various Climates and Pavement Structures 43

3.2. Calculation of the Effective Equivalent Linear Temperature Gradient 46

3.2.1. Nonlinear Temperature Gradient 46

3.2.2. Equivalent Linear Temperature Gradient 46

3.2.3. Effective Equivalent Linear Temperature Gradient 50

3.3. Guidelines for Determining the Temperature Gradients 51

3.3.1. Correlation for the Prediction of EELTG 51

3.3.2. Inputs for the Correlation 53

3.4 Procedure to Calculate EELTG 57

3.5. Summary on PCC Temperature Gradient Characterization 58

4. CONCLUSIONS 58

ACKNOWLEDGEMENT ..... **Error! Bookmark not defined.**

REFERENCES 60

APPENDIX 63

LIST OF FIGURES

Figure 1: Monthly Average Mid-Depth HMA Temperature (MAMDHT) at the MnROAD and Elk River Whitetopping Sections..... 7
Figure 2: Ambient temperature Vs monthly average mid depth HMA layer temperature (MAMDHT) at MnROAD. 9
Figure 3: Annual Mean Daily Average Temperature Map of USA..... 10
Figure 4: Monthly Average HMA Mid-Depth Temperature at the Seven Geographical Locations. 14
Figure 5: Testing Setup for Determining the HMA Resilient Modulus (Loulizi et al., 2006). 15
Figure 6: HMA Resilient Modulus in Different Seasons in MnROAD Whitetopping Cells. 16
Figure 7: HMA Resilient Modulus in Different Seasons in the Selected Seven Geographical Locations. 16
Figure 8: Testing set up for dynamic modulus test (Loulizi et al., 2006). 17
Figure 9: Comparison of resilient modulus and dynamic modulus for SM – 9.5 A mix..... 18
Figure 10: Comparison of resilient modulus and dynamic modulus for BM – 25.0 mix 18
Figure 11: Master Curves for HMA Mixtures for Different Geographical Locations. 22
Figure 12: HMA Dynamic Moduli and Resilient Moduli at Different Temperatures. 23
Figure 13: Effective Length Concept within the Pavement System (ARA, 2004). 24
Figure 14: Effective Length Calculation using Transformed Thickness (ARA, 2004). 24
Figure 15: Loading Frequency for Possible Range of Whitetopping Overlays. 26
Figure 16: Sensitivity of HMA thickness to the loading frequency. 27
Figure 17: Sensitivity of PCC thickness to the loading frequency. 27
Figure 18: Sensitivity of HMA stiffness to the loading frequency. 28
Figure 19: Sensitivity of Subgrade Stiffness to the loading frequency. 28
Figure 20: Sensitivity of PCC thickness to the loading frequency only at 35 mph. 29
Figure 21: Sensitivity of PCC thickness to the loading frequency only at 55 mph. 29
Figure 23: Predictability test of the Adjustment factor regression models. 36
Figure 24: Predictability test of the $EHMA(Ref)$ regression models. 39
Figure 25: Procedure to generate the effective equivalent linear temperature gradient. 42
Figure 26: Locations of the Selected Weather Stations (The background map is the Google Map of the US as of June, 2010). 44

Figure 27: Frequency of Elevations of the Selected Weather Stations. 44
Figure 28: Comparison of the stresses using the strain-equivalent linear temperature gradient and the actual temperature profiles in predicting critical stresses, for 4-in overlay in Champaign, IL. 48
Figure 29: Comparison of the hourly ELTGs using the strain-equivalency approach and the direct-subtraction approach, for 6-in overlay in Champaign, IL. 49
Figure 30: Comparison of the hourly ELTGs between using the strain-equivalency approach and the direct-subtraction approach, for a 4 in overlay in Champaign, IL. 49
Figure 31: Variation in prediction of the EELTG using Equations (29) and (29) for the pavement sections in the database used in this study. 52
Figure 32: Annual concentrating solar resource map of the US in 2009 (http://www.nrel.gov/gis/solar.html, as in May 2010). 54
Figure 33: Statistics on the percentage of sunshine for the weather stations in each zone. 55
Figure 34: Frequency of the annual mean percentage of sunshine for Zones 1 and 2. 55
Figure 35: Frequency of the annual mean percentage of sunshine for Zones 3 and 4. 56
Figure 36: Frequency of the annual mean percentage of sunshine for Zones 5 and 6. 56
Figure 37: Variation in prediction of the EELTG using Equations (28) and (29) for the pavement sections in the database used in this study, using with the recommended zonal values for the percentage of sunshine. 57
Figure 38: Prediction of the EELTG using Equations (28)and (29) for the 4-in pavement sections in Champaign, Illinois, using the zonal average for the percentage of sunshine. ..... **Error! Bookmark not defined.**
Figure 39: Prediction of the EELTG using Equations (28) and (29) for the 6-in pavement sections in Denver, Colorado, using the recommended zonal values for the percentage of sunshine. (observed range in CO: -2 to 6 °F/in) ..... **Error! Bookmark not defined.**

LIST OF TABLES

Table 1: Temperature difference/gradient used by current whitetopping design methods. 3
Table 2: Summary of the design features for the MnROAD and Elk River whitetopping cells. ... 6
Table 3: Ambient Temperature Details for the Seven Geographical Locations. (Source: http://cdo.ncdc.noaa.gov/cgi-bin/climaps/climaps.pl?directive= quick_results&subrnum=&pop=YES, accessed on January, 2010). 10
Table 4: Monthly Mean Daily Average Temperature (MMDAT) for the Seven Geographical Locations. (Source: http://www.ncdc.noaa.gov/oa/climate/online/ccd/meantemp.html, ... 11
Table 5: Design Inputs of the Typical Whitetopping Section Employed by the EICM 12
Table 6: Aggregate Gradation of the Typical HMA Mixture. 21
Table 7: Binder Grade Selection Parameters. 21
Table 8: PG Binder Grades and Viscosity Parameters for the Seven Zones. 21
Table 9: Variables Considered in Full Factorial Study for Loading Frequency in Whitetopping.26
Table 10: Whitetopping Design Features and Material Properties in the Fatigue Analysis. 32
Table 11: Hourly Truck Traffic Distribution Recommended in the MEPDG (ARA, 2004). **Error! Bookmark not defined.**
Table 12:: Regression Coefficients for HMA Modulus Adjustment Factor Equations 35
Table 13: Recommended T_{norm} for each AMDAT Zone 36
Table 14: Regression Coefficients for Reference Month HMA Modulus Equations 37
Table 15: Recommended $TMid - DepthRef$ for each AMDAT Zone 39
Table 16:: Coefficients for EELTG regressions based on slab size 53
Table 17: Typical values for the annual mean percentage sunshine for each zone. 56

1. INTRODUCTION

There are two primary effects of climate on the performance of ultra-thin whitetopping (UTW) and thin whitetopping (TWT), namely the variation of the resilient modulus of the underlying hot mixed asphalt (HMA) with temperature and the development of temperature gradients within the Portland cement concrete (PCC) overlay slabs. First, a method will be developed to account for the climate on changes in HMA stiffness and then the temperature gradients that develop in these bonded overlays will be quantified.

The damage prediction for the whitetopping overlay varies significantly with the underlying HMA stiffness. The magnitude of the critical stress for the overlay, as well as the accumulated fatigue damage, increases with decreasing HMA stiffness. The stiffness of HMA is known to decrease with increasing temperature; therefore, higher levels of fatigue damage are expected in warmer, summer months. Findings from the Task 2 Report (Mu and Vandenbossche, 2010) provide practical evidence of this hypothesis and found that incorporating the temperature dependence of HMA stiffness resulted in significantly higher damage than using a constant stiffness corresponding to an annual mean temperature.

The resilient modulus of HMA is kept constant in most alternative whitetopping design procedures, regardless of current temperature. (Mu and Vandenbossche, 2010). Therefore, there is a need to quantify how the HMA modulus changes seasonally and hourly, and what factors significantly affect the HMA temperature or modulus change for different locations and climatic conditions. The seasonal and hourly variation of HMA stiffness is accounted for here by taking the following steps.

(i) Determining the factors that affect the seasonal and daily HMA temperature (mid-depth HMA temperature) change;
(ii) Developing a database of mid-depth HMA temperatures using the Enhanced Integrated Climatic Model (EICM) (Larson and Dempsey, 2003) for a range of locations throughout the United States (US);
(iii) Determining the HMA modulus for the selected locations and pavement structures;

(iv) Establishing adjustment factors for the HMA modulus to take into account the effect of the hourly temperature variation on the fatigue of the overlay and the monthly variation of the HMA modulus.

Regarding the EICM, 'it is a one-dimensional coupled heat and moisture flow program that simulates changes in the behavior and characteristics of pavement and subgrade materials in conjunction with climatic conditions over several years of operation' (ARA, 2004). It is capable of predicting the nonlinear temperature profile across the depth of a preselected pavement structure. In order to generate the nonlinear temperature profiles, the EICM requires the climatic conditions of the location of the project, which can be obtained from the climatic files downloadable from the Transportation Research Board website: http://onlinepubs.trb.org/onlinepubs/archive/mepdg/climatic_state.htm. These files contain hourly data consisting of ambient temperature, wind speed, sunshine, precipitation and humidity for over 800 weather stations across the country.

The temperature gradient is a significant contributor to stress generation in the PCC overlay. It results in curling of the slabs and thus magnifies the load-induced stresses and accelerates the accumulation of fatigue damage. A positive effective temperature gradient where the top of the slab is warmer than the bottom of the slab results in loss of support at midslab. This condition results in higher stresses and a more rapid accumulation of fatigue damage at the bottom of the slab when truck loads are located near the center of the slab. When a large negative effective temperature gradient is present and the top of the slab is cooler than the bottom of the slab, this results in loss of support at the slab edges and corners. In this instance, heavy axle loads applied simultaneously to each end of the slab result in higher stresses and more rapid accumulation of fatigue damage at the top of the slab.

Although whitetopping is usually constructed with small slabs (e.g. 4-ft × 4-ft/ 6-ft × 6-ft panels) to decrease the environmental stresses such as those due to temperature gradients, the contribution of environmental stresses in the total design stress considering both environmental and load-related stresses is still significant. According to Mu and Vandenbossche (2010), 5- to 30-percent of the total design stress is contributed by the temperature gradient within the PCC

overlay. This ultimate contribution in a given situation is a function of the magnitude and frequency of the temperature gradients as well as the slab dimensions.

Given the significance of the temperature gradient in stress predictions, its establishment in the alternative design procedures is relatively poorly guided. This is more effectively illustrated in Table 1. In Table 1, it can be observed that the sign of the critical temperature gradients is not the same for all the current design procedures. For designers wishing to utilize these procedures, the alternative design procedures provide little to no guidance on establishing site specific temperature gradients. Furthermore, when typical values are suggested, these values are based on localized measurements that might not be applicable everywhere. Based on the previous two statements it becomes immensely important to develop a guideline for establishing the temperature gradients, and subsequently to incorporate the guideline into the BCOA-ME (whitetopping) design procedure.

Table 1: Temperature difference/gradient used by current whitetopping design methods.

Whitetopping design methods	Critical temperature difference/gradient considered
Colorado Department of Transportation (Tarr et al., 1998)	Positive temperature gradient, -1 to 5 °F/in, based on Colorado test measurements
New Jersey Department of Transportation (Gucunski, 1998)	Positive temperature difference, no guidance in determining this input
Portland Cement Association (Wu et al., 1999)	Negative temperature difference, no guidance in determining this input
Illinois Center for Transportation (Roesler et al., 2008)	Negative temperature difference, -1.4 °F/in for Illinois based on equivalent damage

To meet these ends, the following steps were undertaken.

(i) Identifying the factors that affect the temperature gradients in the PCC overlay and selecting a range of locations that are representative of these factors throughout the continental (lower 48) United States;

(ii) Populating the database of PCC temperature gradients using the EICM for the predetermined locations and pavement structures;

(iii) Determining the effective temperature gradient required by the whitetopping design procedures for the selected locations and pavement structures.

(iv) Establishing the guideline for calculating EELTGs.

2. CHARACTERIZATION OF HMA MODULUS

This section focuses on the characterization of the HMA modulus. A discussion is provided on the factors that affect the temperature of the HMA layer. The relationship between the ambient temperature and the HMA layer temperature is also established in this section, which facilitated a zonal division of the country based on the annual mean daily average temperature (AMDAT) (ambient temperature). Using the AMDAT, the temperature dependency of the HMA modulus is then investigated based on the temperature data from the field test sections. Finally, adjustment factors are proposed to account for the effect of the seasonal as well as hourly temperature variation on the HMA modulus.

2.1. Factors affecting the HMA Temperature

The daily or seasonal temperature variation of an HMA layer in a whitetopping structure is different from a conventional flexible pavement. Because the HMA layer is under a PCC overlay, factors like solar radiation, humidity and wind speed do not have a significant effect on the seasonal variation of the HMA temperature. Based on this statement, it is a reasonable assumption that, the HMA temperature should only be a function of the PCC overlay thickness, the HMA thickness, the climatic condition and the geographical location. To investigate the effect of these important parameters, the HMA temperature data for the whitetopping sections at the Minnesota Road Research Facility (MnROAD) on I-94, and at Elk River on US-169 is analyzed.

MnROAD is a full-scale pavement test facility consisting of a 3.5-mile section of Interstate 94 and a 2.5-mile low-volume roadway near Albertville, Minnesota, approximately 35 miles northwest of Minneapolis. The MnROAD Facility contains more than 50 pavement designs, defined as cells, with each test cell typically being between 100 and 500-ft in length. Six different sections (Cells 92 through 97) received a whitetopping overlay in 1997. Among these sections, Cells 93, 94 and 95 were replaced by Cells 60, 61, 62 and 63 in 2004 because of an excessive drop in serviceability. New whitetopping sections, Cells 114 through 914, were placed in 2008. All of these test cells were s constructed on the interstate portion of MnROAD,

referred to as the mainline, and are/were subjected to live interstate traffic redirected from westbound traffic on I-94.

Ultra-thin whitetopping test sections were also constructed in 1997 at three consecutive intersections on US-169 in Elk River, Minnesota. These overlays were constructed in the outer southbound lane of US-169 at the intersections of Jackson (Cell 98), School (Cell 99), and Main Streets (Cell 91). The design features of the MnROAD (I-94) and Elk River (US-169) whitetopping sections are presented in Table 2. The MnROAD and Elk River whitetopping projects are immensely important to research in the area of bonded concrete overlays. A large number of cells in these sections were heavily instrumented with thermocouples and strain gauges at various key locations. Temperature data was collected at different depths of the PCC overlay and the HMA layer.

The main differences between the MnROAD and Elk River projects are the thickness and the condition of the existing HMA layer. The thickness of the PCC overlay in the MnROAD cells ranges from 3 to-6 inches, while the thickness was 3-in for all three Elk River cells. MnROAD cells were constructed on top of a 7 to 10-in thick of sound HMA layer, unlike Elk River cells, which were constructed on top of a severely distressed 3-in thick HMA layer. Because of the poor condition of the 3-in thick HMA layer and the heavy traffic on the road, the Elk River project survived for only two years.

It was initially anticipated that key design features such as the thickness of the PCC and HMA layers affected the relationship between the HMA temperature and the most influential climatic factors such as ambient temperature. To better understand this interaction, temperature data from the whitetopping cells at MnROAD and Elk River, was analyzed. The selected cells in Table 2 present all the combinations of both thin and ultra-thin PCC overlays on top of both thick and thin HMA layers.

Table 2: Summary of the design features for the MnROAD and Elk River whitetopping test cells.

	Cell No.	Age	PCC slab thickness (in)	HMA layer thickness (in)	Type	Slab size (ft × ft)
MnROAD	92	Oct 97-Apr 10	6	7	TWT	10 × 12
	93	Oct 97-Oct 04	4	9	UTW	4 × 4
	94	Oct 97-Oct 04	3	10	UTW	4 × 4
	95	Oct 97-Oct 04	3	10	UTW	5 x 6
	96	Oct 97-Current	6	7	TWT	5 x 6
	97	Oct 97-Apr 10	6	7	TWT	10 x 12
	60	Oct 04-Present	5	7	TWT	5 x 6
	61	Oct 04-Present	5	7	TWT	5 x 6
	62	Oct 04-Present	4	8	UTW	5 x 6
	63	Oct 04-Present	4	8	UTW	5 x 6
	114	Oct 08-Present	6	5	TWT	6 × 6
	214	Oct 08-Present	6	5	TWT	6 × 6
	314	Oct 08-Present	6	6	TWT	6 × 6
	414	Oct 08-Present	6	6	TWT	6 × 6
	514	Oct 08-Present	6	7	TWT	6 × 6
	614	Oct 08-Present	6	7	TWT	6 x 12
	714	Oct 08-Present	6	7.5	TWT	6 × 6
	814	Oct 08-Present	6	8	TWT	6 × 6
	914	Oct 08-Present	6	8	TWT	6 × 6
Elk River	98	Sept 97-Sept 99	3	3	UTW	4 × 4
	99	Sept 97-Sept 99	3	3	UTW	4 × 4
	91	Sept 97-Sept 99	3	3	UTW	6 × 6

Temperature data at multiple depths through the HMA layer was measured using thermocouples with a 15-min recording interval. Although temperature data was available at multiple depths throughout the asphalt layer, only the temperature at the mid depth of the HMA layer was used to represent the effective temperature for the HMA layer. Based on previous research (Inge et al., 1995 and Kim et al., 1995), the use of the mid-depth HMA temperature is adequate to characterize the temperature in the asphalt layer and for relating temperature to stiffness. Utilizing this observation, the monthly average mid-depth HMA temperature (MAMDHT) was obtained in order to consider the seasonal variation of the HMA temperatures and its effect on the HMA modulus.

Figure 1 shows the MAMDHT for four of the whitetopping cells at MnROAD and Elk River. The temperature data available for Cells 93 and 97 represent the data from 1998 to 2002,

and for Cell 95 the data represents the period between 1997 and 2002. Cell 98, on US-169, has less data and only consists of temperatures from 1998. Within the data from Cell 98 in 1998, temperature data for the months of March, April, and December is incomplete. Because of this limitation, the average temperature for these three months could not be included in Figure 1. Using the data from Figure 1 the effects of design features and seasons were investigated with the results being elaborated upon in the following sections.

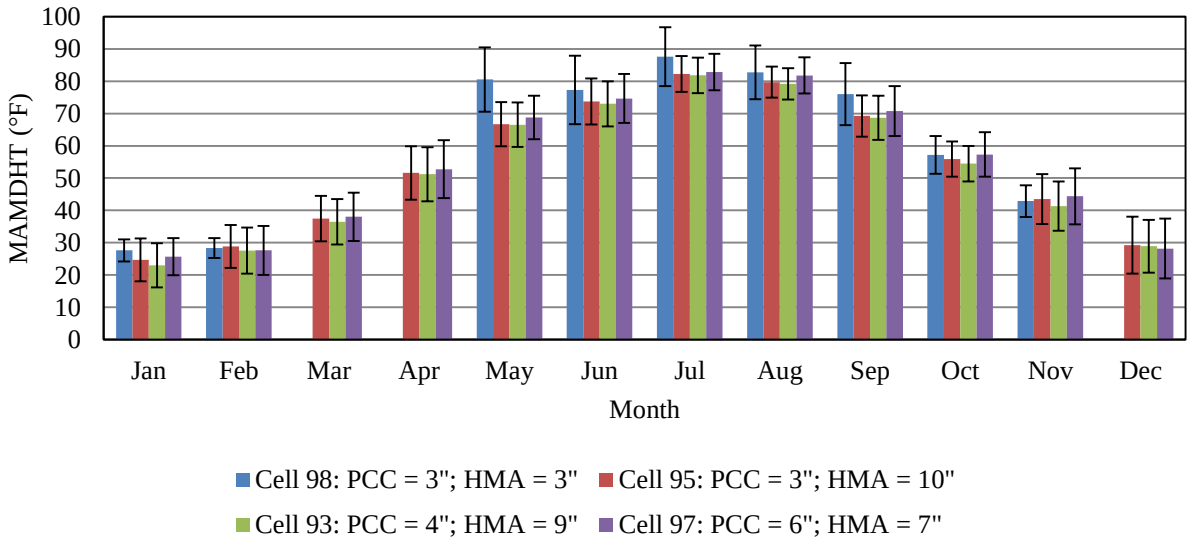

Figure 1: Monthly Average Mid-Depth HMA Temperature (MAMDHT) at the MnROAD and Elk River Whitetopping Sections.

2.1.1. Effect of PCC Layer Thickness

A closer observation of the MAMDHTs in Figure 1, for cells with 3, 4 and 6-inch thick PCC overlays reveals that the average temperature, in a given month, does not differ by a considerable magnitude. Cell 98, which has a 3-in thick PCC overlay, experienced a marginally higher MAMDHT for a few months in the spring and summer, but practically, the variation is within the standard deviation of the mid depth temperatures for a given month. The standard deviations of the MAMDHTs for the three MnROAD cells also appear to be different by a negligible amount. This observation indicates that the HMA mid-depth temperature is not a function of the PCC overlay thickness and instead is more a function of the environmental conditions.

The reason for the low sensitivity of MAMDHT to the PCC thickness could be the comparatively smaller thickness of the whitetopping slabs. Based on the analysis of one-year of temperature data, Vandenbossche (2001) reported that the mean temperature gradient for 3, 4 and 6-inch MnROAD whitetopping cells are -0.90, -0.91 and -0.7 °F/in, respectively. This means that the temperature differences between the top and bottom of the slab for those cells are 2.7, 3.6 and 4.2 °F, respectively. Therefore, it can be concluded that the temperature difference between the top and the bottom of a whitetopping overlay with thickness of 3-6 inches is negligible compared to the standard deviation of the temperatures in a given month or even in a day.

2.1.2. Effect of HMA Layer Thickness

Figure 1 also indicates a negligible effect of the HMA layer thickness for almost the entire period of the year. Although the midpoint of the HMA layer in Cell 98, Elk River (3-in HMA layer under a 3-in PCC layer) is 4.5 in from the surface of the PCC overlay as opposed to 8 to 9.5-in for the MnROAD cells (10-in HMA under 3-in PCC or 7-in HMA under 6-in PCC), the MAMDHTs for all the cells are similar in all the months, except May. A closer examination of the MAMDHTs between Cells 98 and 95 for the month of May indicates that Cell 98 experienced an approximately 12 °F higher MAMDHT during this month. Although the actual reason is unknown, a relatively warmer subgrade for the thinner HMA layer in the transition period of May (from winter to summer) could possibly explain this observation.

2.1.3. Effect of Seasons

The seasonal variation of the HMA layer temperature is clearly visible in Figure 1. It can be observed that the HMA temperature is the highest in the month of July and the lowest in January. Since the temperature of the HMA layer under the whitetopping overlay does not significantly depend on factors like, solar radiation, wind speed and humidity; a great correlation between the ambient temperature and the HMA temperature can be anticipated.

To understand the relationship between the ambient temperature and the HMA temperature, the monthly mean daily average ambient temperatures at the MnROAD project location (Minneapolis) are drawn against the MAMDHTs for Cells 95 (3-in PCC over 10-in

HMA) and 93 (4-in PCC over 9-in HMA) as shown in Figure 2. It is not surprising to observe that the ambient temperature and MAMDHT follow a similar trend. The polynomials in Figure 2, which were generated based on second order polynomial best fit, further serve to highlight this point. From Figure 2 it can be observed that there is a good correlation between the HMA mid depth temperature and the ambient temperature and that the seasonal variation of the MAMDHT is related to the seasonal variation of the ambient temperatures.

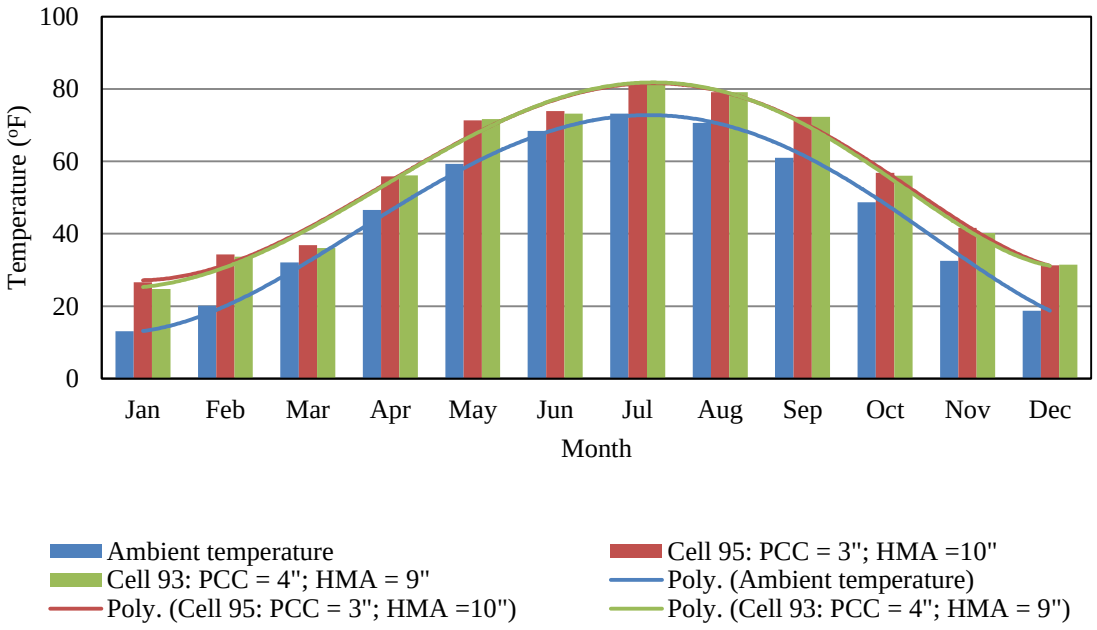

Figure 2: Ambient temperature Vs monthly average mid depth HMA layer temperature (MAMDHT) at MnROAD.

2.1.4. Effect of Geographical Location (Climate)

In order to characterize the HMA temperature in different parts of the country, a zonal division of the country was carried out with respect to the ambient temperature. Using National Oceanic and Atmospheric Administration (NOAA) data for the annual mean daily average temperature (AMDAT), the entire continental US states (lower 48) was divided into seven different climatic zones using a 5°F interval of AMDAT. The resulting zonal distribution map is presented in Figure 3.

For analysis of the influence of climate, one weather station was selected to represent each zone. These selected weather stations can be seen in Table 3 along with the latitude,

longitude, and the annual mean daily average, minimum, and maximum temperatures. Monthly mean daily average temperatures (MMDAT) of the representative locations were also obtained as presented in Table 4. Of the seven geographical locations, Minneapolis (AMDAT: 32.1-40 °F) and Miami (AMDAT: 60.1-70 °F) are the two extremes with respect to AMDAT.

Table 3: Ambient Temperature Details for the Seven Geographical Locations. (Source: http://cdo.ncdc.noaa.gov/cgi-bin/climaps/climaps.pl?directive=quick_results&subrnum=&pop=YES, accessed on January, 2010).

Zone	Location of representative weather station	Latitude	Longitude	Annual mean daily average temperature (°F)	Annual mean daily minimum temperature (°F)	Annual mean daily maximum temperature (°F)
1	Minneapolis, MN	44.53	-93.14	40.1-45.0	32.1-40	50.1-60
2	Erie, PA	42.05	-80.11	45.1-50.0	32.1-40	50.1-60
3	Champaign, IL	40.02	-88.17	50.1-55.0	40.1-45	60.1-65
4	Chattanooga, TN	35.02	-85.12	55.1-60.0	45.1-50	65.1-70
5	Tuscaloosa, AL	33.13	-87.37	60.1-65.0	50.1-55	70.1-75
6	Dallas, TX	32.41	-96.52	65.1-70.0	55.1-60	75.1-80
7	Miami, FL	25.49	-80.18	>70.0	60.1-70	>80.10

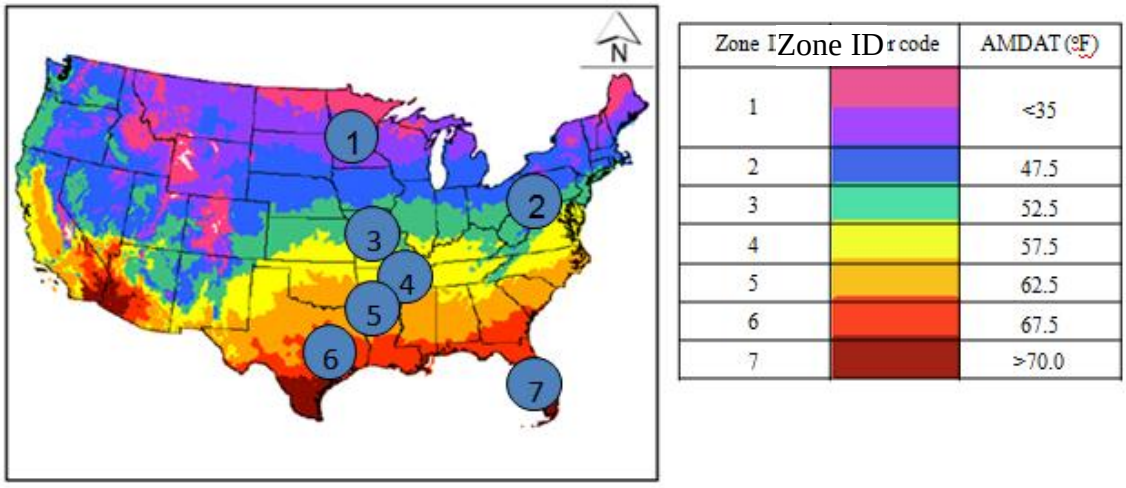

Figure 3: Annual Mean Daily Average Temperature Map of USA.
(Source: http://cdo.ncdc.noaa.gov/climaps/temp0313.pdf, accessed on January, 2010).

Table 4: Monthly Mean Daily Average Temperature (MMDAT) for the Seven Geographical Locations. (Source: http://www.ncdc.noaa.gov/oa/climate/online/ccd/meantemp.html, accessed on January, 2010)

Zone	Location	Jan	Feb	Mar	Apr	May	Jun	July	Aug	Sep	Oct	Nov	Dec
1	Minneapolis, MN	13.1	20.1	32.1	46.6	59.3	68.4	73.2	70.6	61.0	48.7	32.5	18.7
2	Erie, PA	26.9	28.2	36.5	46.8	58.1	67.4	72.1	70.9	64.0	53.3	42.9	32.7
3	Champaign, IL	22.0	27.0	37.3	47.8	58.7	68.2	73.3	71.7	63.8	52.1	39.3	27.4
4	Chattanooga,TN	39.4	43.4	51.4	59.6	67.7	75.4	79.6	78.5	72.1	60.4	50.3	42.4
5	Tuscaloosa, AL	42.6	46.8	54.5	61.3	69.3	76.4	80.2	79.6	73.8	62.9	53.1	45.6
6	Dallas, TX	44.1	49.4	57.4	65.0	73.1	80.9	85.0	84.4	77.5	67.2	55.1	46.7
7	Miami, FL	68.1	69.1	72.4	75.7	79.6	82.4	83.7	83.6	82.4	78.8	74.4	69.9

For the selected geographical locations, the EICM was utilized to predict the mid-depth HMA temperature on an hourly interval with the pavement structure and geographical location given as inputs. The EICM uses geographical location as an input to obtain weather data for a given location. In this instance weather data from a nearby weather station was used directly, however, for locations that are distant from weather stations used in the database, interpolation can be done to obtain a site specific climatic file. In this study, the climatic data for all seven stations is available at http://onlinepubs.trb.org/onlinepubs/archive/mepdg/climatic_state.htm.

Using the EICM an HMA mid-depth temperature was predicted for a typical whitetopping pavement section constructed in each zone. The need to repeat this step to compare multiple pavement structures was unnecessary because of the conclusion from the last section that the HMA mid-depth temperature has negligible variation with changes in the PCC and HMA layer thicknesses. Based on these conclusions, a typical 4-in PCC overlay on top of an 8-in HMA layer was adopted as the standard pavement structure.

Additional details pertaining to the pavement structure include that the HMA layer in the adopted typical whitetopping section sits on top of a 10-in asphalt treated base course placed on an American Association of State Highway and Transportation Officials (AASHTO) A-6 subgrade. The design features of the typical whitetopping section, material properties and other input parameters employed into the EICM program are presented in Table 5.

Table 5: Design Inputs of the Typical Whitetopping Section Employed by the EICM

PCC material inputs	
Thickness of layer (in)	4
Number of elements in the layer	4
Thermal conductivity (BTU/hr-ft-°F)	1.25
Heat capacity (BTU/lb-°F)	0.28
Total unit weight (pcf)	150
HMA material inputs	
Thickness of layer (in)	8
Number of elements in the layer	4
Thermal conductivity (BTU/hr-ft-°F)	0.67
Heat capacity (BTU/lb-°F)	0.22
Total unit weight (pcf)	148
Base course	
Type	Asphalt treated
Thickness of layer (in)	10
Number of elements	2
Porosity	0.19
Saturated permeability (ft/hr)	1180
Dry unit weight (pcf)	136.8
Dry thermal conductivity (BTU/hr-ft-°F)	0.8
Dry heat capacity (BTU/ft^3-°F)	0.22
Maximum dry unit weight (pcf)	136.8
Specific gravity	2.70
Saturated hydraulic conductivity (ft/hr)	1.18×10^3
Optimum gravimetric water content (%)	7.1
Degree of saturation (%)	82.8
Aggregate gradation	Default
Initial volumetric water content (%)	15.57
Soil water characteristic curve parameter	Default
Subgrade	
Type	A-6
Number of elements	2
Porosity	0.36
Saturated permeability (ft/hr)	1.95×10^{-5}
Dry unit weight (pcf)	107.90
Dry thermal conductivity (BTU/hr-ft-°F)	0.80
Dry heat capacity (BTU/ft^3-°F)	0.22
Initial volumetric water content (%)	29.57
Specific gravity	2.70
Saturated hydraulic conductivity (ft/hr)	1.95×10^{-5}
Optimum gravimetric water content (%)	17.1
Degree of saturation (%)	82.1
Soil water characteristic curve parameter	Default

Many of the input parameters are default values. Thermal conductivity and heat capacity of the concrete were determined as the national average values recommended in the Mechanistic-Empirical Pavement Design Guide (MEPDG) (ARA, 2004). For the surface shortwave absorptivity, Roesler et al. (2008) suggested that a value of 0.65 should be appropriate when a white sealant is applied. The upper temperature limit of the freezing range (32 °F) and the lower temperature limit of freezing range (30.2 °F) were kept the same for all the EICM runs. With the inputs established and using an analysis period of one year, the temperature data consisting of the mid-depth HMA temperature was generated on an hourly basis.

Based on the hourly mid-depth temperature data generated by the EICM, the MAMDHT and the standard deviation of the hourly temperatures for that given month were obtained for all seven zones, as presented in Figure 4. As anticipated, the variation in the monthly HMA temperature (Figure 4) is similar to the variation in the monthly ambient temperature (Table 4) for all seven locations. For example, the two locations that present the extreme ambient temperatures, namely Minneapolis, MN and Miami, FL are also the locations where extreme HMA mid-depth temperatures can be found. Through further examination of Figure 4, it is found that the difference in the magnitude of MAMDHTs between the seven locations appears to be more significant in the winter season than the summer season. This is exemplified by the fact that the difference in MAMDHT between Minneapolis and Miami is 34 °F in January and 10 °F in July. The seasonal variation of the MAMDHT in the northern states also appears greater than the southern states. For example, the maximum difference in MAMDHTs (July Vs. December) in Minneapolis is 56 ^{o}F compared to 25 ^{o}F in Miami.

Based on the analysis presented above, it can be concluded that the season of the year and the locations of the project play the most important roles in determining the magnitude of the MAMDHT. Therefore, in whitetopping design, a different MAMDHT, and hence a different value of HMA resilient modulus, should be used for each month and location.

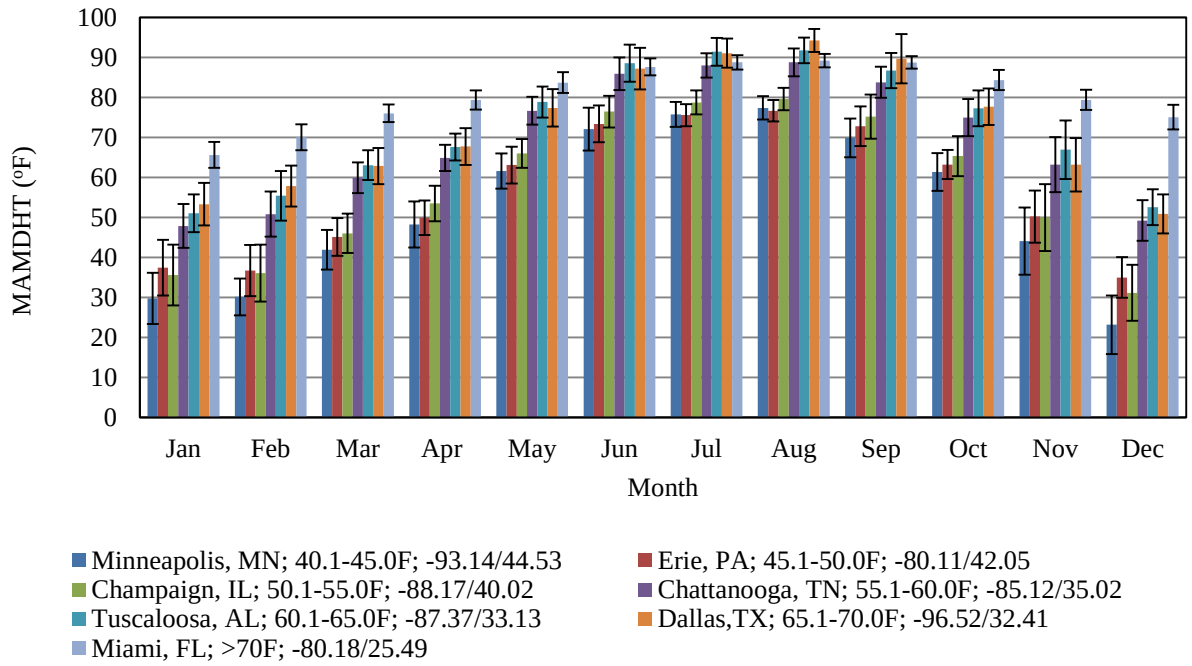

Note: Each legend represents location, state, AMDAT (°F), longitude and latitude (degree).

Figure 4: Monthly Average HMA Mid-Depth Temperature at the Seven Geographical Locations.

2.2. Characterization of HMA Modulus

HMA modulus is one of the key input parameters required in the mechanistic design of whitetopping. Before the construction of whitetopping, the HMA layer modulus can be backcalculated using either nondestructive testing equipment such as a Falling Weight Deflectometer (FWD) test, or through testing retrieved pavement cores in the laboratory. HMA modulus can be characterized either by resilient modulus or by dynamic modulus. As shown in Figure 5, in the case of resilient modulus, the laboratory test is performed on a cylindrical specimen by applying haversine loading pulses along its vertical diametric plane according to the American Society of Testing Materials (ASTM) D 4123 specification. For the testing setup depicted in Figure 5, the resilient modulus is defined as the ratio of the applied stress to the recoverable axial strain.

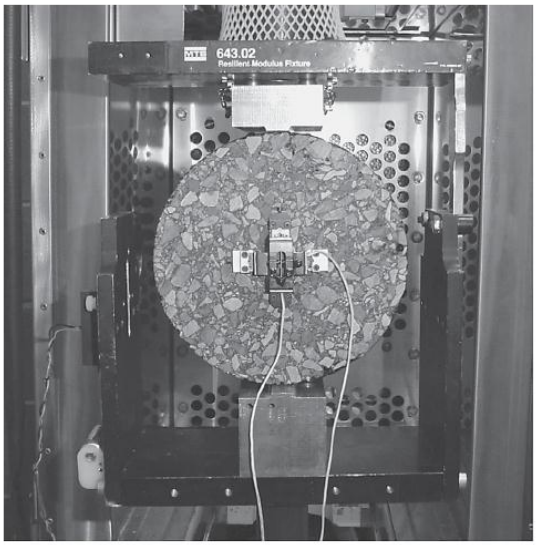

Figure 5: Testing Setup for Determining the HMA Resilient Modulus (Loulizi et al., 2006).

In a study by Vandenbossche and Fagerness (2002), a load duration of 0.1 sec and rest period of 1 sec was used for the resilient modulus test on specimens from MnROAD. The relation between the HMA resilient modulus and the temperature was established as shown in Equation (1).

$$E_{HMA} = 205.65 \cdot T^2 - 36132 \cdot T + 1730000 \quad (1)$$

where T is the temperature ,°F and E_{HMA} is the HMA resilient modulus, psi.

This relationship was then used to define the relationship between the HMA resilient modulus and the temperature for the MnROAD whitetopping sections, as shown in Figure 6. The difference in the HMA resilient modulus among MnROAD cells for a given month is negligible since the mid-depth HMA temperature is relatively constant between the cells for that month. The HMA resilient moduli for the seven weather stations, including the one in Minneapolis, MN that is close to the MnROAD site, were also determined using the Vandenbossche and Fagerness model (Vandenbossche and Fagerness, 2002) as presented in Figure 7. Comparing Figure 6 and Figure 7, it can be seen that the HMA resilient modulus determined for the MnROAD cells closely matches the modulus determined using the temperatures generated using the EICM and the Minneapolis weather station. These results

indicate a good predictability of the mid-depth HMA temperature using the EICM, since the same equation was used to calculate the HMA modulus for the temperatures measured at MnROAD and the temperatures predicted using the EICM.

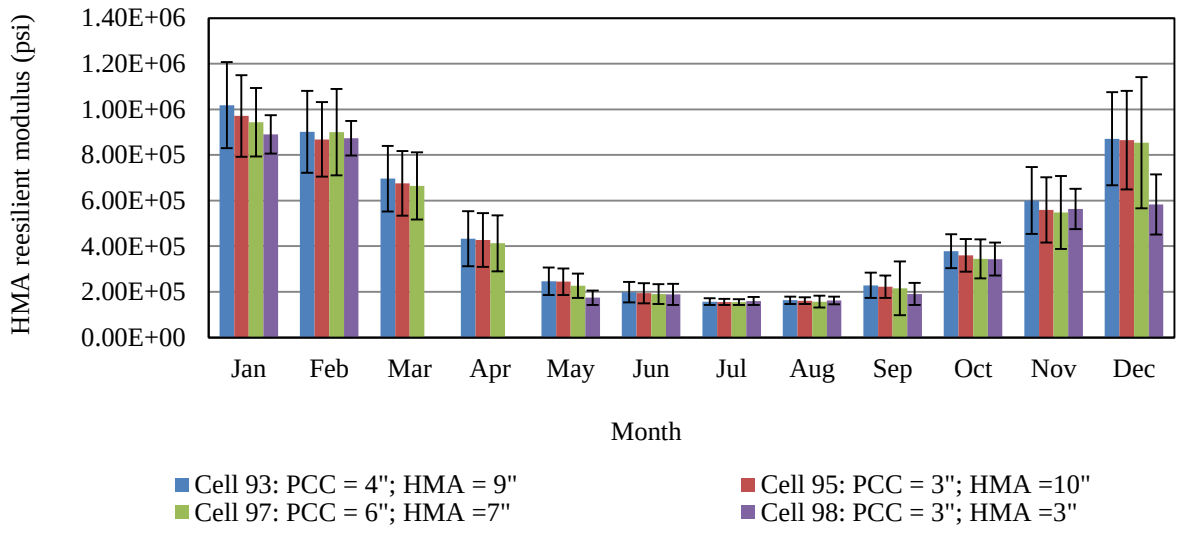

Figure 6: HMA Resilient Modulus in Different Seasons in MnROAD Whitetopping Cells.

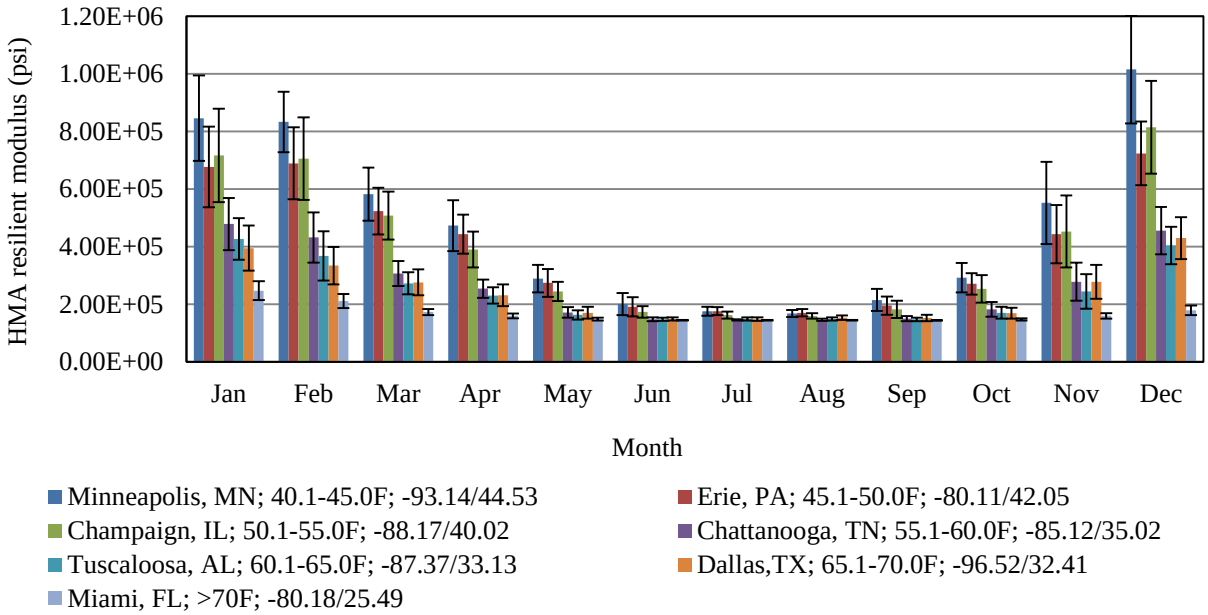

Figure 7: HMA Resilient Modulus in Different Seasons in the Selected Seven Geographical Locations.

It might be inadequate to use Equation (1) that was established based on MnROAD data to predict the HMA modulus for other states. To address this issue, site-specific master curves (ARA, 2004) were employed to predict the HMA dynamic modulus. The dynamic modulus of HMA is a complex number that relates stress to strain for a cylindrical specimen subjected to a sinusoidal vertical loading. The advantage of a dynamic modulus test over a resilient modulus test is that the dynamic modulus test provides a better characterization of HMA than the resilient modulus, because it provides full characterization of the mix over different temperature and loading frequencies (Loulizi et al., 2006). Figure 8 presents a test set up for the dynamic modulus test. The American Association of State Highway and Transportation Officials (AASHTO) pavement design procedure (1993) incorporated the resilient modulus value to characterize the HMA layer, whereas, the MEPDG (ARA, 2004) replaces the resilient modulus by the dynamic modulus. Although dynamic modulus is adopted by a few new design procedures, the application of the resilient modulus is still promising because of a simple test procedure. In fact dynamic modulus and resilient modulus is interchangeably used sometime. Loulizi et al. (2006) has conducted a comparative study to investigate the correlation between these two parameters. In their study, two different mixes of HMA, such as a surface mix (SM – 9.5A) and a base mix (BM – 25.0) were designed in accordance with the Superpave specifications.

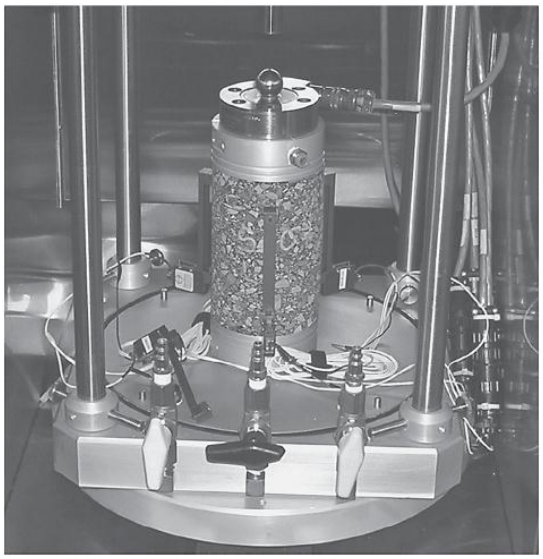

Figure 8: Testing set up for dynamic modulus test (Loulizi et al., 2006).

The correlation between the HMA resilient modulus and dynamic modulus for the two adopted mixes obtained in their study is presented in Figure 9 and Figure 10. The interesting discovery of that study was the confirmation of a linear relationship between resilient modulus and dynamic modulus at 5 Hz. frequency. In the case of the surface mix, the resilient modulus and dynamic modulus is almost similar (7% difference). But for the base mix, dynamic modulus is 40 percent higher than the resilient modulus.

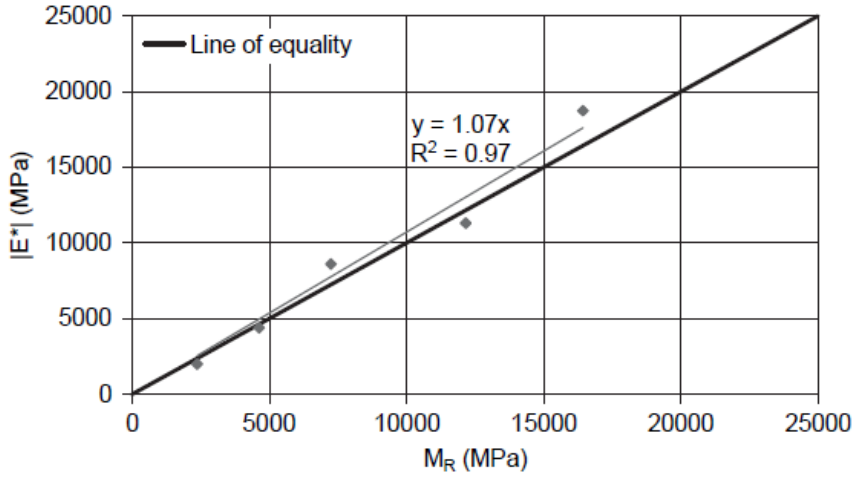

E* = Dynamic modulus; M_R = Resilient modulus; 1 MPA = 145 psi

Figure 9: Comparison of resilient modulus and dynamic modulus for SM – 9.5 A mix (Loulizi et al., 2006).

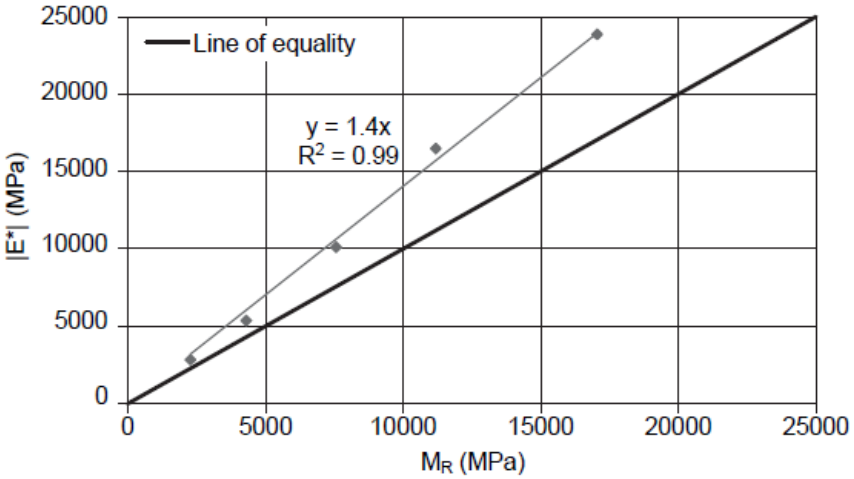

Figure 10: Comparison of resilient modulus and dynamic modulus for BM – 25.0 mix (Loulizi et al., 2006).

A master curve is a nonlinear sigmoidal function that has the form given in Equations (2) through (4) and that describe the dependency of the HMA modulus on the loading frequency and temperature. Based on the master curve, the predicted dynamic modulus will vary with the HMA mixture because of the variation in the asphalt binder properties between geographical zones. Within each zone, however, the asphalt used remains relatively constant.

$$log|E^*| = \delta + \frac{\alpha}{1 + e^{(\beta+\gamma(\log(t_r))}} \quad (2)$$

$$t_r = \frac{t}{a(T)} \quad (3)$$

$$\log(t_r) = \log(t) - log[a(T)] \quad (4)$$

where E^* is the dynamic modulus, psi; t_r is the time of loading at the reference temperature, s; δ, α are the fitting parameters for a given set of data; δ represents the minimum value of E^* and $\delta + \alpha$ represents the maximum value of E^* and β, γ are the parameters describing the shape of the sigmoidal function.

The fitting parameters δ and α depend on the aggregate gradation, binder content and air void content, whereas β and γ depend on the characteristics of the asphalt binder and the magnitude of δ and α; t_r is the time of loading at the reference temperature, s; t is the time of loading at a given temperature of interest, s; $a(T)$ is the shift factor as a function of temperature; T is the temperature of interest, Rankine. The other parameters can be calculated by using the following equations:

$$\delta = 3.750063 + 0.029232\rho_{200} - 0.001767\rho_{200}^2 - 0.002841\rho_4 - 0.058097V_a - 0.82208\left[\frac{Vb_{eff}}{Vb_{eff} + V_a}\right] \quad (5)$$

$$\propto = 3.871977 - 0.0021\rho_4 + 0.003958\rho_{38} - 0.000017\rho_{38}^2 + 0.005470\rho_{34} \quad (6)$$

$$\beta = -0.603313 - 0.393532log(\eta_{T_r}) \quad (7)$$

$$\log(t_r) = \log(t) - c(log(\eta) - log(\eta_{T_r})) \quad (8)$$

$$\gamma = 0.313351; c = 1.255882 \quad (9)$$

where η is the bitumen viscosity, 10^{6} poise; V_a is the air void content, percent; V_{beff} is the effective bitumen content, percent by volume; ρ_{34} is the cumulative percent retained on the ¾ in sieve; ρ_{38} is the cumulative percent retained on the 3/8 in sieve; ρ_4 is the cumulative percent retained on the No. 4 sieve and ρ_{200} is the percent passing the No. 200 sieve.

The binder viscosity, η is a function of the binder type and the temperature as recommended by the ASTM viscosity temperature relationship (ASTM D 2493). This relationship can be formulated as shown in Equation (10).

$$\log\log\eta = A + VTS\log T_R \tag{10}$$

where η is the viscosity of binder, centi poise; T_R is the temperature, Rankine, A is the regression intercept and VTS is the regression slope of viscosity temperature susceptibility. The values of A and VTS are a recommended function of the asphalt binder grade. It may be worth noting that Equation (10) is only recommended for unaged asphalt binder, whereas the binder of the HMA underneath a whitetopping overlay is almost always aged. Nevertheless, Equation (10) still provides decent service in establishing the relationship between the HMA temperature and its dynamic modulus.

In this study, the aggregate gradation (see in

Table 6), binder quantity (12.5% by volume of the mix) and air void percentage (5.8%) were assumed as same for the HMA mixtures used in the seven zones. This typical aggregate gradation was selected referring to the statistics of large numbers of HMA mix design examples in Appendix CC of MEPDG documentation (ARA, 2004) so that it represents a well range of the HMA mixes that are in use in the country. Coincidently, this HMA mix is also almost similar to the HMA mix used in a HMA pavement section (Cell 33) in MnROAD (Clyne et al., 2003). This cell was constructed with Performance Grade (PG) 58-28 binder.

Table 6: Aggregate Gradation of the Typical HMA Mixture.

Sieve size	Percent finer
1 in	100
¾ in	100
3/8 in	88
No. 4	70
No. 200	4.3

The asphalt Performance Grade (PG) for the selected zones were obtained using the SHRP LTPPBIND version 3.1 (Pavement System LLC, 2005) which is a Superpave binder selection program developed for the Federal Highway Administration (FHWA). In this program, the asphalt binder grade is correlated with the geographical information (i.e. longitude, latitude and elevation of the project site), depth to the surface of HMA layer, traffic characteristics and the desired reliability level. In this study, all the parameters except the geographical location are kept similar for all the seven zones as presented in Table 7. The recommended PG grades and corresponding values of *VTS* and *A* are given in Table 8. It can be seen that the grades of the asphalt binder for the last three weather stations (Tuscaloosa, AL; Dallas, TX; Miami, FL) are the same so that a single master curve is able to represent these three locations.

Table 7: Binder Grade Selection Parameters.

Depth to surface of HMA layer	4 in
Desired reliability	98%
Traffic speed category	Slow
Anticipated equivalent standard axle load (ESAL)	3 to 10 million

Table 8: PG Binder Grades and Viscosity Parameters for the Seven Zones.

Location	PG grade	VTS	A
Minneapolis	58-28	-3.701	11.010
Erie	52-22	-4.342	12.755
Champaign, IL	58-22	-3.981	11.787
Chattanooga, TN	64-16	-3.822	11.375
Tuscaloosa, AL	64-10	-3.842	11.432
Dallas, TX	64-10	-3.842	11.432
Miami, FL	64-10	-3.842	11.432

Figure 11 shows the five master curves that represent the seven selected geographical locations. It is interesting to see that the trend of the variation of dynamic modulus with respect

to the reduced frequency (1/ reduced time) are quite similar for all the locations.. A close observation reveals that the dynamic moduli value in southern states is marginally higher than the northern states, for a given frequency, which is reasonable since a more viscous asphalt binder is generally used in the southern states.

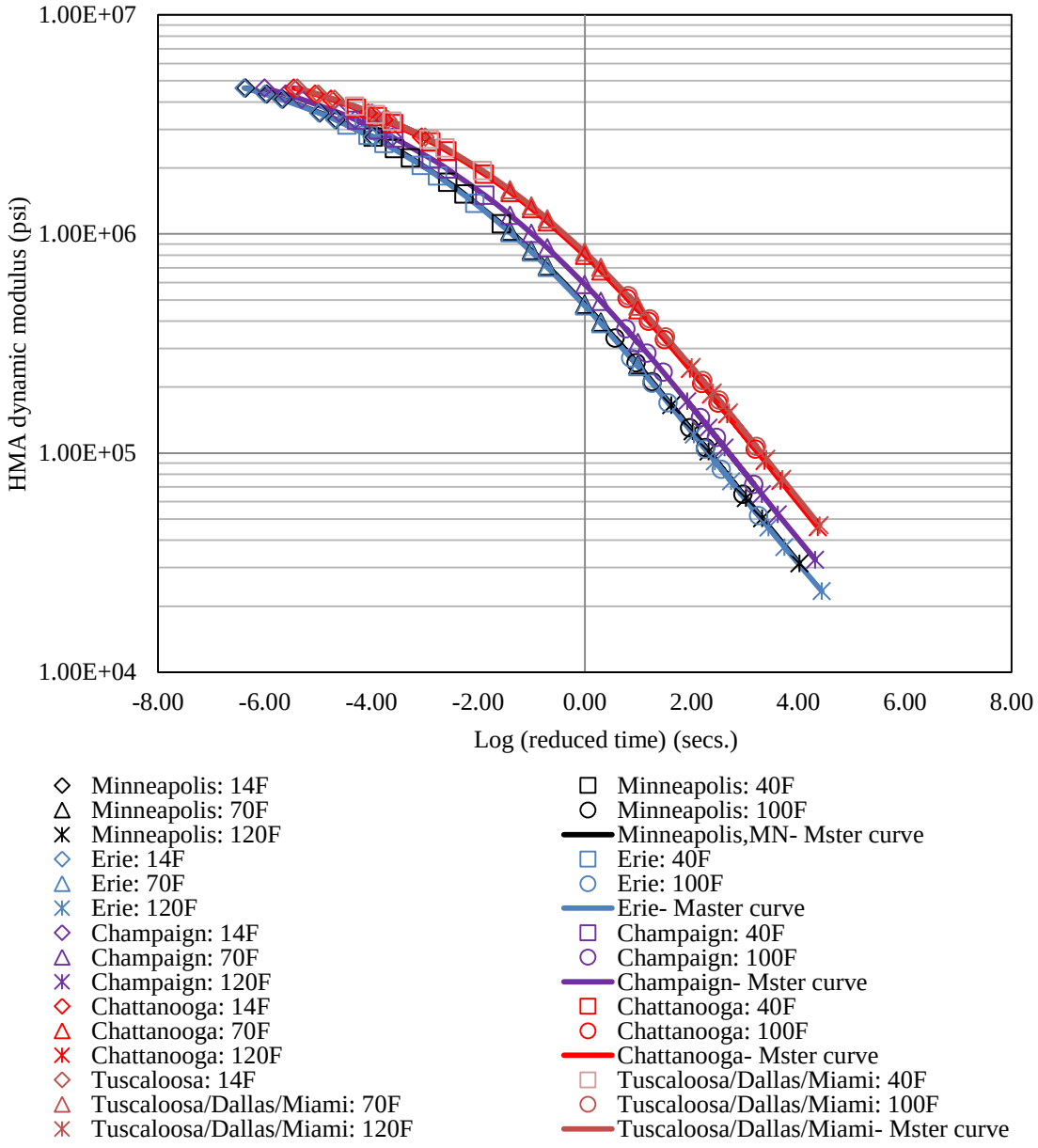

Figure 11: Master Curves for HMA Mixtures for Different Geographical Locations.

The variation of the dynamic modulus with temperature for all seven locations is plotted in Figure 12 . All the dynamic modulus values were obtained with a loading time of 0.1 sec (10 Hz. Frequency). This loading time is considered in study because it basically simulates the typical vehicle speed on the whitetopping overlays in the country.

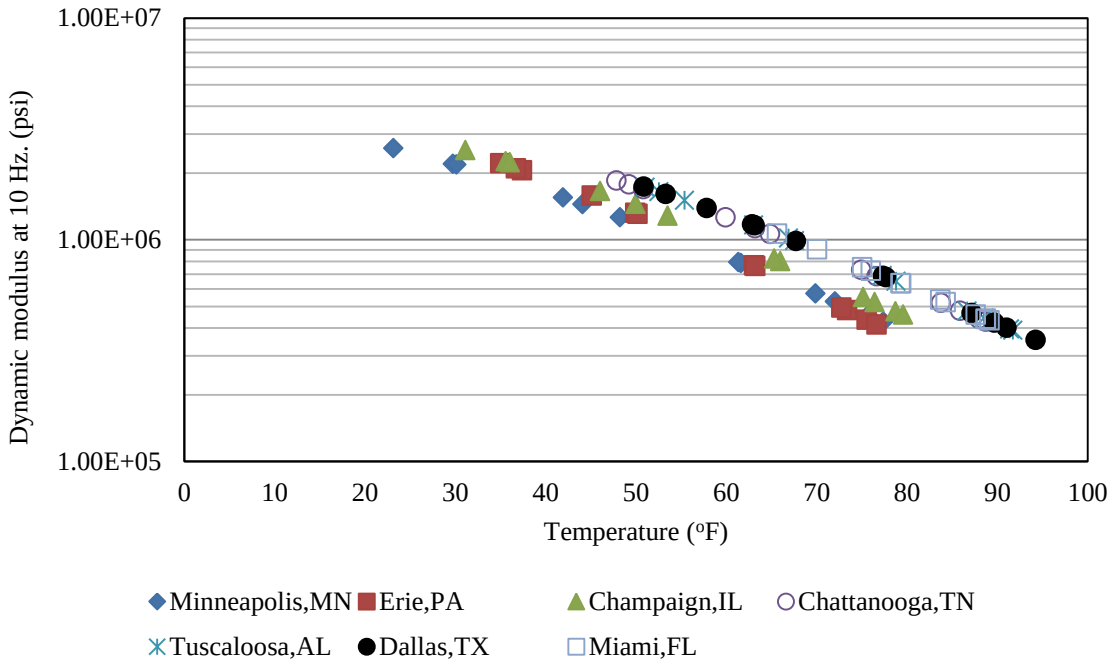

Figure 12: HMA Dynamic Moduli and Resilient Moduli at Different Temperatures.

In the MEPDG (ARA, 2004), it is suggested that the loading time should be calculated based on the effective length of the load pulse that varies with the depth and the operational speed of the vehicles, as shown in Equation (11).

$$t = \frac{L_{eff}}{17.6\, v_s} \tag{11}$$

Where t is the time of load, sec; $L_{eff}$is the effective length of the load pulse, inches; and v_s is the velocity, mph. The magnitude of L_{eff} is function of radius of loading area, a_c, depth of the layers and moduli of the layers as is illustrated in Figure 13 and Figure 14. It can be seen that the angle of load dispersion is wider at the upper layers which are generally stiffer compared to the lower layers. However, using Odemark's equivalent thickness method (ARA, 2004), as illustrated in Figure 14, one can find out the magnitude of L_{eff} at any depth of the pavement

system after transforming all layers into an equivalent single layer. In this case, L_{eff} is computed at an equivalent depth, Z_{eff} which can be determined by using Equation (12).

$$Z_{eff} = \sum_{i=1}^{n-1} \left(h_i \sqrt[3]{\frac{E_i}{E_{SG}}} \right) + h_n \sqrt[3]{\frac{E_n}{E_{SG}}} \tag{12}$$

Where h_n is the thickness of the layer of interest (layer n). The value of n depends on the location of the layer of interest in the pavement system. If the effective depth is needed at the mid-depth of the second layer in the pavement structure, then n = 2. The variables, h_i, E_i are the thicknesses and moduli of the layers above the layer of interest, whereas, E_{SG} is the modulus of the subgrade.

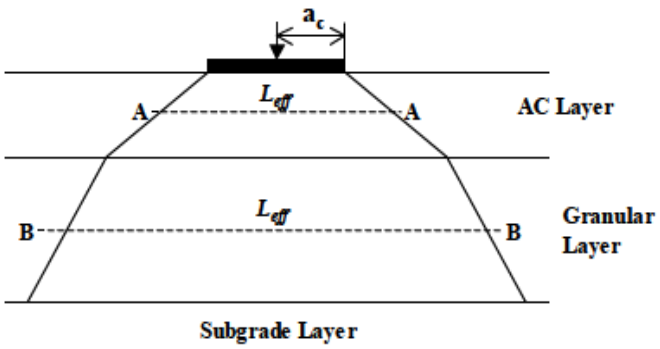

Figure 13: Effective Length Concept within the Pavement System (ARA, 2004).

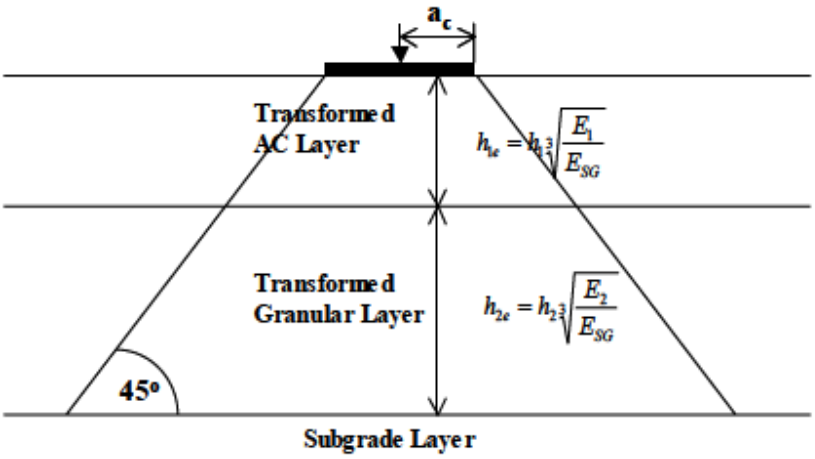

Figure 14: Effective Length Calculation using Transformed Thickness (ARA, 2004).

Once the magnitude of Z_{eff} is determined, then based on the vehicle axle configuration, L_{eff} can be computed. For single axle load configuration, L_{eff} can be computed by Equation (13).

$$L_{eff} = 2\left(a_c + Z_{eff}\right) \tag{13}$$

In whitetopping, the PCC overlay generally possesses a higher magnitude of modulus of elasticity and distributes the load to a wider area as a result. Even though it is not purely a valid assumption that whitetopping acts like a layered system, when PCC and HMA layers are transformed to a single layer with subgrade equivalent stiffness, then the above relationship for time of loading and L_{eff} can be assumed to be applied. The L_{eff} at the mid-depth of the HMA layer under a whitetopping overlay can then be determined using this Equation (13).

$$L_{eff} = 2\left(a_c + \left(h_{PCC}\sqrt[3]{\frac{E_{PCC}}{E_{SG}}} + \frac{h_{HMA}}{2}\sqrt[3]{\frac{E_{HMA}}{E_{SG}}}\right)\right) \tag{14}$$

To determine the typical loading frequency in the whitetopping overlays, a full factorial study is then carried out for a wide range of possible types of whitetopping. The parameters considered in the study can be found in Table 9. The loading frequency computed for each case considered in this study is plotted together in Figure 15. The sensitivity of each parameter to the loading frequency is then studied as shown in Figure 16 through Figure 21. It is interesting to observe that in most of the cases the loading frequency varies from 5 to 15 Hz. Moreover, only PCC thickness is found to be sensitive to the loading frequency. Other parameters, namely, HMA thickness, HMA modulus and the subgrade modulus are marginally or not sensitive to the loading frequency. In Figure 20, it can be seen that the frequency for 3- or 4-inch concrete overlays is around 10 Hz. The frequency for 6-in overlays is around 5 Hz. However, it should be noted that this is the result from an operational speed of 35 mph. This should be mostly encountered for applications of UTW. For TWTs, on the other hand, the operational speed should be assigned as 55 mph instead. In Figure 21, it is obviously that 10 Hz should be used as the main frequency for thicker slabs. In conclusion, it is recommended that 10 Hz be used as the

design frequency for the calculation of mid-depth HMA dynamic modulus using the master curve.

Table 9: Variables Considered in Full Factorial Study for Loading Frequency in Whitetopping.

Subgrade modulus, ksi (AASHTO type)	HMA modulus, ksi (Season)	PCC modulus, ksi	PCC thickness, in	HMA thickness, in	Half of the tire print length, in	Operational speed, mph
15 (A-6) 30 (A-1)	200 (Summer) 600 (Spring) 1500 (Winter)	4000	2, 3, 4, 5, and 6	3, 4, 5, 6, 7, 8, and 9	5	35

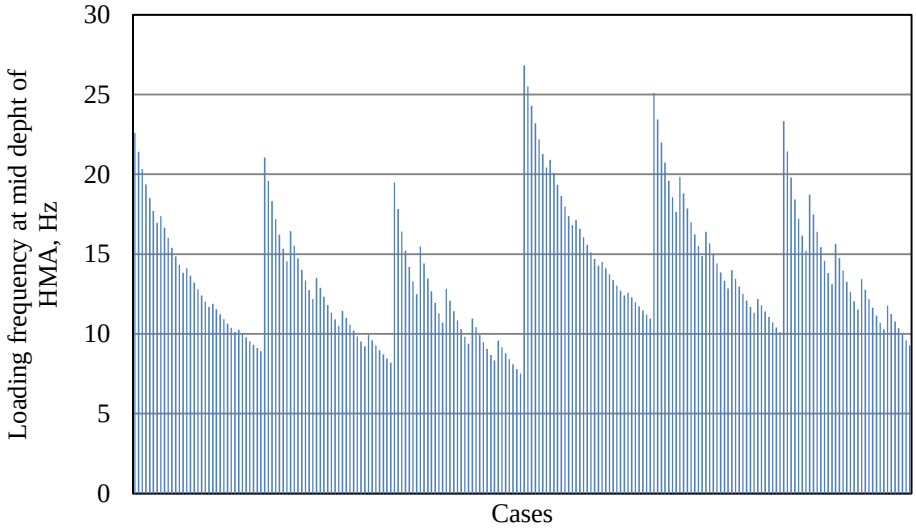

Figure 15: Loading Frequency for Possible Range of Whitetopping Overlays.

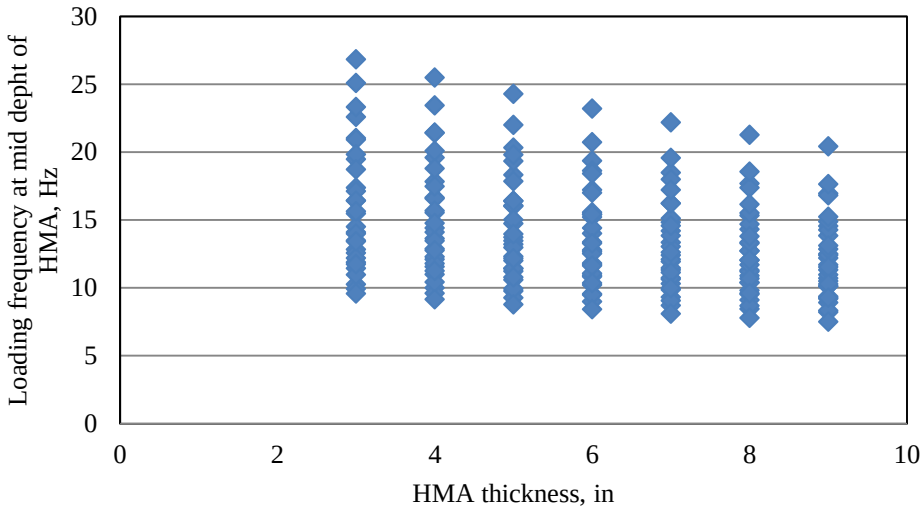

Figure 16: Sensitivity of HMA thickness to the loading frequency.

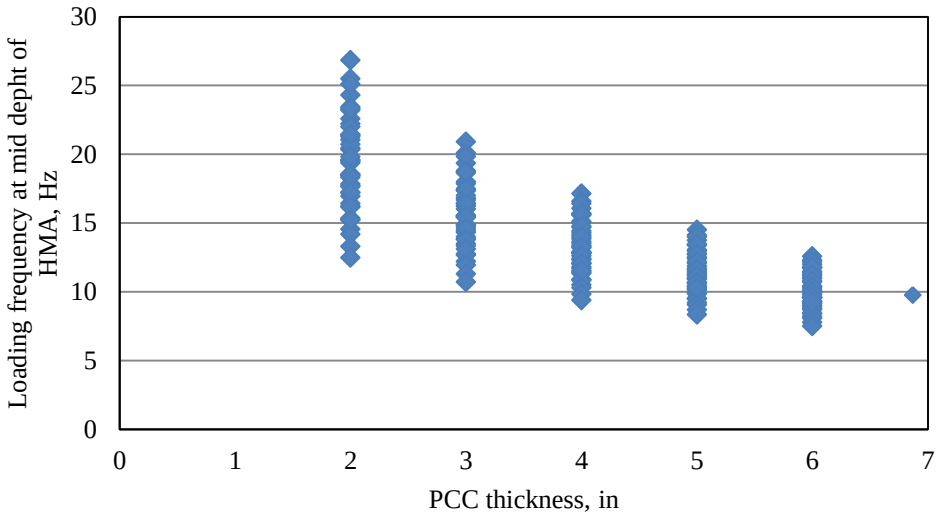

Figure 17: Sensitivity of PCC thickness to the loading frequency.

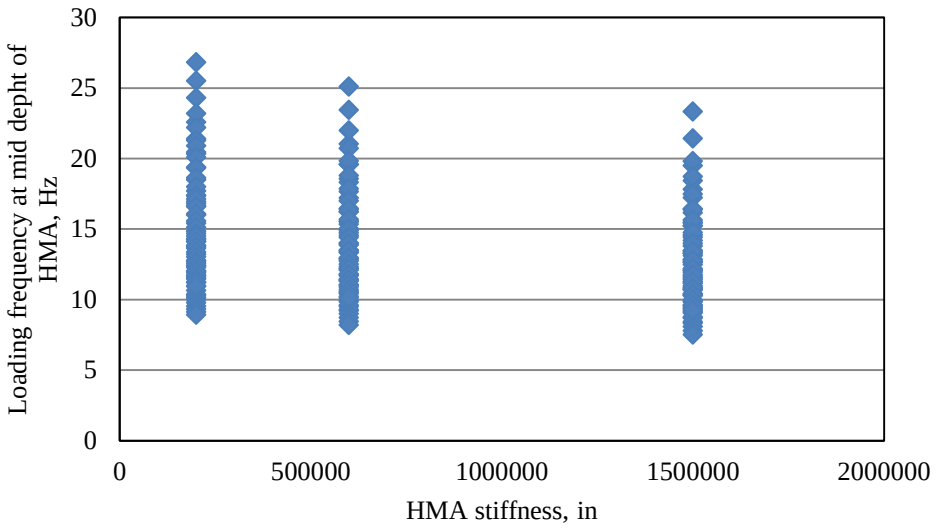

Figure 18: Sensitivity of HMA stiffness to the loading frequency.

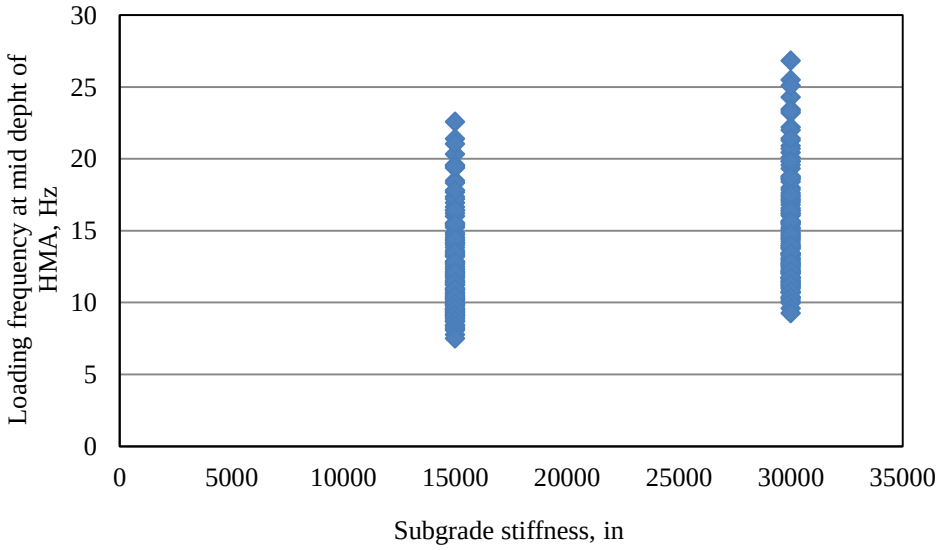

Figure 19: Sensitivity of Subgrade Stiffness to the loading frequency.

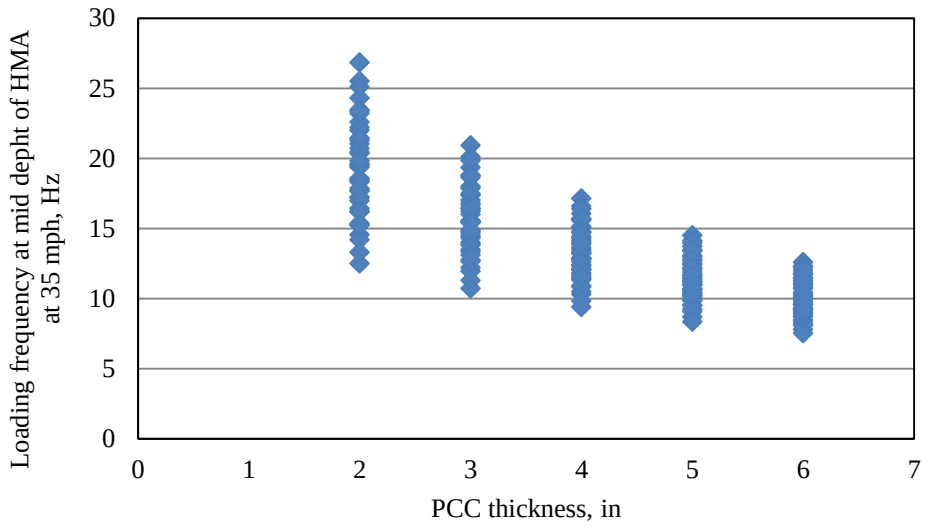

Figure 20: Sensitivity of PCC thickness to the loading frequency only at 35 mph.

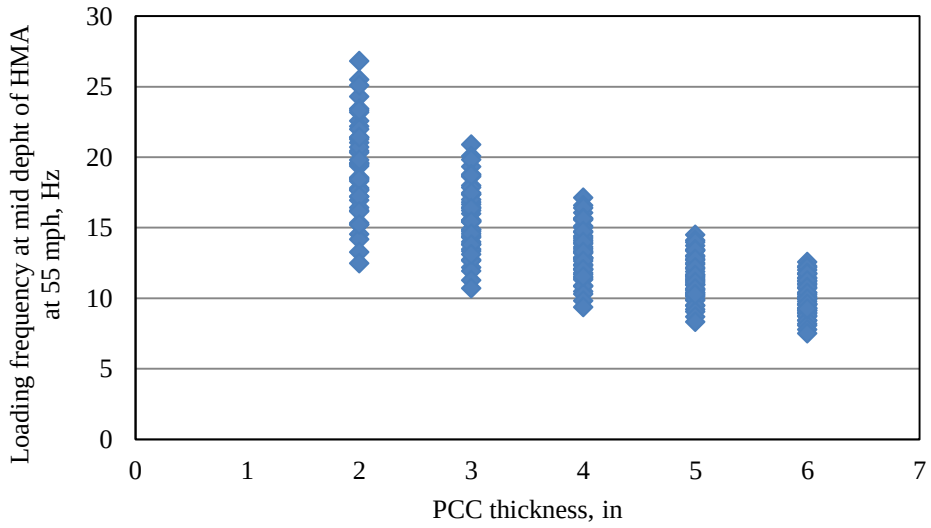

Figure 21: Sensitivity of PCC thickness to the loading frequency only at 55 mph.

2.3 Considerations in Establishing Effective HMA Modulus Values

Section 2.1.4 concluded that a different value of HMA Modulus should be used for each month and location. The locations can be grouped according to the 7 AMDAT Zones due to the relationship found between mid-depth HMA Temperature and the ambient temperature in Section 2.1.3. However, a method needs to be employed to obtain the monthly effective HMA Modulus values.

The framework to establish effective HMA Modulus values for use in design involves generating a database of hourly mid-depth HMA temperatures that are populated with numerous EICM runs that include a large range of climatic conditions and whitetopping structures. By expanding the number of climatic stations used in the analysis to include significantly more than one station per AMDAT zone, a greater range of climatic conditions can be captured resulting in a more robust prediction. The hourly mid-depth HMA temperatures are then used to generate hourly HMA Modulus values with the aid of the master curve as outlined in Section 2.2. Through fatigue equivalency, effective HMA Modulus values are calculated for each month.

The use of the twelve effective HMA Modulus values when applied throughout the design life results in the same fatigue damage as if hourly HMA Modulus values were used in an hourly fatigue analysis. The twelve effective monthly HMA Modulus values can then be normalized to a reference month to obtain adjustment factors (F) that account for seasonal variation of the HMA modulus in addition to the effect of the hourly temperature variation on the fatigue of the overlay. The details for establishing the Effective HMA Modulus values are outlined in the following sections.

2.3.1 Populating Database of Mid-Depth HMA Temperature for Various Climates

A large database of weather stations were chosen to incorporate all climatic conditions present in the continental (lower 48) United States. 194 weather stations were selected as shown in Table A1 of the Appendix. The stations selected are shown in Figure 22. The Average Monthly Daily Average Temperature (AMDAT) Zones were determined for each of the stations so that the locations could be easily grouped for analysis to determine HMA Modulus adjustment factors.

For each weather station, hourly climatic conditions over a one-year period were obtained for ambient temperature, mid-depth HMA temperature, wind speed, sunshine, precipitation, and relative humidity. This hourly climatic data, along with material property inputs, are required by the EICM to calculate the hourly temperature profiles to populate the required database. The hourly temperature profiles can then be used to obtain mid-depth HMA temperature and the temperature gradient in the PCC overlay. In addition to calculating the temperature profiles, statistical indicators such as the mean and standard deviation of the hourly climatic features were

computed over the one-year period for each station to aid in the comparison of the results from the analysis. These statistics are presented in Table A2 in the Appendix.

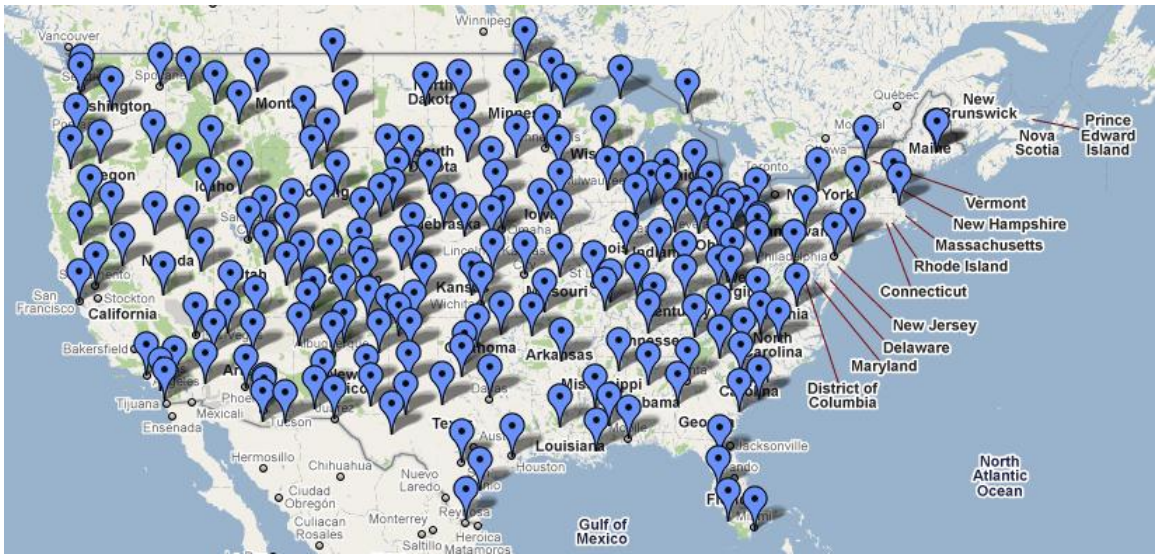

Figure 22: Locations of the selected weather stations (The background map is the Google Map of the US as of June, 2010).

2.3.2 Structural Models Used in Fatigue Analysis

Since corner cracking is the dominant distress in whitetopping with small size panels such as 3-ft x 3-ft and 4-ft x 4-ft, the ACPA structural model was used for predicting the stresses. The slabs with joint spacing less than or equal to 4.5 ft consider corner cracks as the primary distress. The structural models were used to predict the stress in the whitetopping with 6-ft x 6-ft panels. For slabs with joint spacing greater than 4.5 ft and less than or equal to 7 ft, the structural model is modified from the Colorado structural model to include a stress adjustment factor that accounts for partial bonding. For slabs with a longitudinal joint spacing greater than 7 ft and a standard transverse joint spacing of 12 ft, the structural model is also modified from the Colorado structural model.

2.3.3 Fatigue Analysis Variables

Fatigue consumption of the whitetopping overlay is a function of design features, material properties, and design traffic. A preliminary analysis identified four most significant design variables to include in this fatigue analysis, namely the HMA thickness, the PCC thickness, the overlay slab size and the PCC modulus of rupture (MOR). The whitetopping

design variables and materials properties selected for the fatigue analysis are presented in Table 10. The three methods used, based on three different slab sizes, utilized different sets of design features. Analysis for the smallest slabs, those with joint spacing less than or equal to 4.5 ft, used two PCC thicknesses and two HMA thicknesses. The mid size slabs, those with joint spacing greater than 4.5 ft and less than or equal to 7 ft (modified from the Colorado method) used three PCC thicknesses and two HMA thicknesses. Finally, the largest slab size, those with a longitudinal joint spacing greater than 7 ft, utilized two PCC thicknesses and three HMA thicknesses in the analysis. Additionally, for the smallest slabs, 3-ft and 4-ft square panel sizes were used while only 6-ft square panels were assumed for the mid size slabs, and only 10 ×12 ft panels were used for the largest slabs. The other inputs, such as the modulus of subgrade reaction (k), coefficient of thermal expansion (CTE) of concrete and Poison's ratios of HMA and concrete that have negligible effect on the fatigue predictions, were assumed as constant. The elastic modulus values of the concrete were correlated based upon the PCC modulus of rupture values that were assumed. All the values of HMA moduli were determined developing master curves for each weather station. Temperature gradients used in the stress prediction by both the ACPA and the Colorado methods are determined based on the EICM predicted temperatures. Negative temperature gradients that are critical for corner cracks (Roesler et al., 2008) and are employed for slabs with a joint spacing less than or equal to 4.5 ft. Positive temperature gradients that are critical for transverse cracks (Sheehan et al., 2004) are employed for slabs with a joint spacing greater than 4.5 ft. Since the analysis in this section focuses on the effect of hourly variation of the temperature on the HMA modulus by looking at the fatigue in the overlay, the influence of temperature gradient in the PCC layer was isolated by using the linear temperature gradient for each hour for both hourly and monthly fatigue calculations.

Table 10: Whitetopping Design Features and Material Properties in the Fatigue Analysis.

Design features in the fatigue analysis			
Joint spacing	PCC layer thickness (in)	HMA layer thickness (in)	Panel size (ft ×ft)
≤4.5 ft	3 and 4	4 and 8	3 × 3 and 4 × 4
>4.5 ft ≤ 7 ft	3, 4, and 6	4 and 8	6 × 6
Longitudinal > 7 ft	5 and 6	4, 6, and 8	10L × 12W
Material Properties			

Concrete MOR (psi)	PCC modulus (10^6 psi)	PCC CTE ($10^{-6}/^0$F)	k (pci)	Poisson's ratio of PCC	Poisson's ratio of HMA
550, 650, and 750	3.5, 4, 4.4	5	200	0.15	0.35

In the fatigue analysis, each hypothetical whitetopping section was loaded with 1 million ESALs. For the analysis using monthly HMA modulus, the total ESALs is assumed to be evenly distributed amongst the twelve months. For the analysis with hourly HMA modulus, the hourly truck traffic distribution that was considered was determined based on the LTPP traffic distribution as shown in **Error! Reference source not found.**1 (ARA, 2004). For the 24 hypothetical whitetopping sections for the smallest slabs and 18 hypothetical whitetopping sections for each the mid-size and larger slabs, two sets of fatigue prediction data were generated for each weather station. One based on monthly average HMA modulus (12 values) and the other based on hourly HMA modulus (12×30×24=8760 values).

Table 11: Hourly Truck Traffic Distribution Recommended in the MEPDG (ARA, 2004).

Time period	Distribution (percent)	Time period	Distribution (percent)
12:00 a.m. – 1:00 a.m.	2.3	12:00 p.m. – 1:00 p.m.	5.9
1:00 a.m. – 2:00 a.m.	2.3	1:00 p.m. – 2:00 p.m.	5.9
2:00 a.m. – 3:00 a.m.	2.3	2:00 p.m. – 3:00 p.m.	5.9
3:00 a.m. – 4:00 a.m.	2.3	3:00 p.m. – 4:00 p.m.	5.9
4:00 a.m. – 5:00 a.m.	2.3	4:00 p.m – 5:00 p.m	4.6
5:00 a.m. – 6:00 a.m.	2.3	5:00 p.m. – 6:00 p.m	4.6
6:00 a.m. – 7:00 a.m.	5.0	6:00 p.m. – 7:00 p.m.	4.6
7:00 a.m. – 8:00 a.m.	5.0	7:00 p.m. – 8:00 p.m	4.6
8:00 a.m. – 9:00 a.m.	5.0	8:00 p.m. – 9:00 p.m.	3.1
9:00 a.m. – 10:00 a.m.	5.0	9:00 p.m. – 10:00 p.m.	3.1
10:00 a.m. – 11:00 a.m.	5.9	10:00 p.m. – 11:00 p.m.	3.1
11:00 a.m. – 12:00 p.m.	5.9	11:00 p.m.– 12:00 a.m.	3.1

2.3.4 Adjustment for HMA Modulus Variation

The fatigue accumulation using the hourly HMA modulus for a certain month is denoted as FA_h, while the fatigue accumulation using the monthly HMA modulus for the same month is FA_m. The difference between FA_h and FA_m indicates the effect of hourly HMA modulus variation. To take into account of this effect, an adjustment to the monthly HMA modulus should be made so that FA_m becomes equivalent to the FA_h. The effective HMA Modulus can be defined as the monthly average HMA modulus that takes into account the hourly variation. The

effective HMA Modulus is obtained through trial and error until the difference between FA_m and FA_h approaches to zero. Hence, one effective HMA Modulus was obtained for each month for a particular whitetopping design, for each weather station in each zone. The twelve effective monthly HMA Modulus values are then normalized to a reference month to obtain adjustment factors (*F*). For this analysis, January is chosen as the reference month and thus the value of *F* for January is one.

2.3.5 Regression Models for HMA Modulus Adjustment Factor

The adjustment factor (*F*) for HMA modulus is a function of pavement design features, month and AMDAT zone. In order to summarize the many adjustment factors so that they can be more readily incorporated in the design procedures, nonlinear regression models are developed for F with respect to the design features for each zone and design procedure. Therefore, all three analysis methods have 7 zonal regressions for a total of 21. *F* is obtained based on fatigue equivalency and thus it shows dependence on seasons (months). The variation of *F* with months can be considered in the regression models by using the normalized mid-depth HMA temperatures. The variation of *F* with location can be considered by partitioning the weather stations into the 7 AMDAT Zones.

Before developing the regression models, the statistical significance of each variable was tested and it was found that the only significant variables on the magnitude of the *F* were the normalized mid-depth HMA temperature and the HMA thickness. In this study, the monthly average mid-depth HMA temperature data was taken from the EICM data and then normalized to the reference month. The developed regression models are summarized below for both methods and all seven zones in Equations **Error! Reference source not found.**) and Table 12.

$$F = C_1 + \frac{C_2}{T_{Norm}} + C_3 * h_{HMA} + C_4 * h_{PCC} \quad (15)$$

where h_{HMA} is the HMA layer thicknesses, inches; and T_{norm} is normalized mid-depth HMA temperature of the project location and h_{PCC} .

Table 12:: Regression Coefficients for HMA Modulus Adjustment Factor Equations

≤ 4.5 ft × 4.5 ft joint spacing	Zone 1	Zone 2	Zone 3	Zone 4	Zone 5	Zone 6	Zone 7
C_1	-0.139	-0.246	-0.300	-0.310	-0.525	-0.654	-0.428
C_2	1.07	1.25	1.32	1.31	1.51	1.66	1.41
C_3	-0.00576	-0.00657	-0.00804	-0.00764	-0.00335	-0.00540	-0.00705
C_4	0	0	0	0	0	0	0
R^2	0.871	0.913	0.892	0.897	0.925	0.944	0.868
> 4.5 ft and ≤ 7 ft joint spacing	Zone 1	Zone 2	Zone 3	Zone 4	Zone 5	Zone 6	Zone 7
C_1	-0.2169	-0.3455	-0.4058	-0.3747	-0.4566	-0.4726	-0.4968
C_2	1.05296	1.1836	1.2773	1.2575	1.4604	1.5751	1.4385
C_3	0.00581	0.00801	0.00434	-0.000016	-0.007	-0.0129	-0.0025
C_4	0.008295	0.0145	0.01658	0.01371	0.00202	-0.0107	0.00429
R^2	0.857	0.798	0.881	0.870	0.912	0.940	0.862
> 7 ft longitudinal joint spacing	Zone 1	Zone 2	Zone 3	Zone 4	Zone 5	Zone 6	Zone 7
C_1	0.09321	0.02420	0.11736	-0.0688	-0.2431	-0.0635	-0.0950
C_2	0.76515	0.85253	0.71162	0.92720	1.0960	0.8516	0.9290
C_3	0.01936	0.025210	0.02728	0.02867	0.02822	0.02641	0.02136
C_4	0	0	0	0	0	0	0
R^2	0.659	0.641	0.563	0.615	0.613	0.652	0.683

High R^2 values for each regression indicates good predictability of the regression models, which can also be seen in **Error! Reference source not found.**3. This plot shows the variation between original adjustment factors and predicted adjustment factors using all of the regression models.

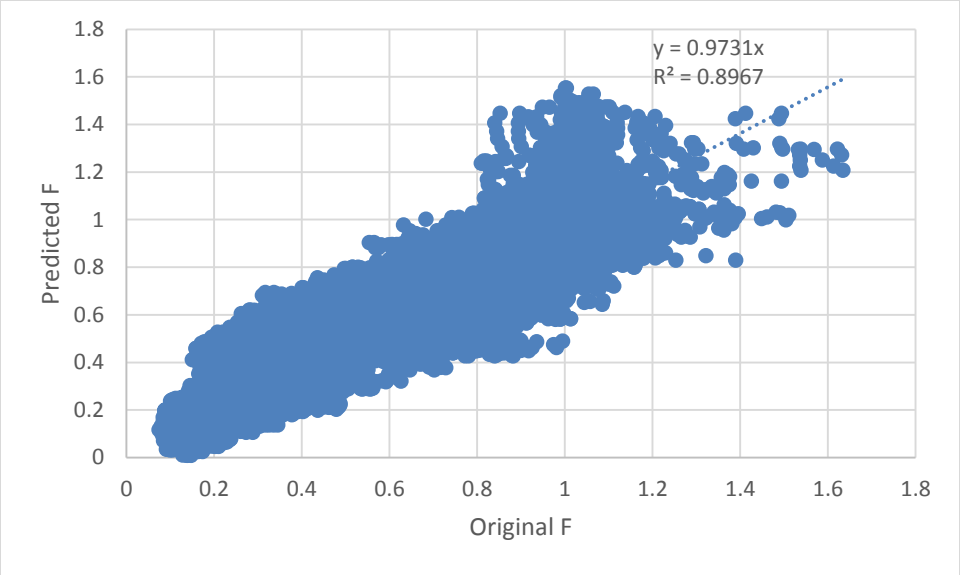

Figure 223: Predictability test of the Adjustment factor regression models.

In summary, *F* can be calculated for each month for each zone using the corresponding regression model, where the HMA thickness and normalized mid-depth HMA temperature should be known. Recommended normalized mid-depth HMA temperatures are provided for each month and AMDAT Zone in Table 13. These values were obtained based upon averages for every weather station used in the study. The adjusted monthly HMA modulus can then be estimated by multiplying the corresponding adjustment factor *F* to the HMA modulus of a reference month. The HMA modulus of January is considered as the reference month in this study. To obtain monthly adjusted HMA modulus based on other reference months, *F* should be updated by normalizing all the adjustment factors by the *F* of the reference month.

Table 13: Recommended T_{norm} for each AMDAT Zone

	Jan	Feb	Mar	Apr	May	Jun	Jul	Aug	Sept	Oct	Nov	Dec
Zone 1	1.00	1.00	1.41	1.88	2.46	2.75	3.00	2.97	2.36	2.03	1.40	0.94
Zone 2	1.00	1.05	1.36	1.82	2.27	2.53	2.72	2.71	2.21	1.92	1.37	0.97
Zone 3	1.00	1.18	1.39	1.82	2.14	2.37	2.52	2.50	2.10	1.86	1.40	1.04
Zone 4	1.00	1.21	1.37	1.78	2.04	2.22	2.35	2.33	1.98	1.78	1.39	1.01
Zone 5	1.00	1.17	1.28	1.51	1.71	1.84	1.92	1.89	1.67	1.51	1.24	1.04
Zone 6	1.00	1.17	1.27	1.51	1.72	1.85	1.92	1.91	1.70	1.54	1.27	1.04
Zone 7	1.00	1.08	1.27	1.39	1.67	1.76	1.86	1.88	1.60	1.46	1.14	1.05

2.3.6 Regression Models for Reference Month HMA Modulus

In addition to the regression models for the adjustment factors, it becomes necessary to develop regression equations for the reference month HMA Modulus to avoid requiring designers to input this value. The reference month HMA Modulus determined from the developed regression equations can then be multiplied with the 12 adjustment factors found from Equation (15) and Table 13 to give effective HMA Modulus values for every month in the calendar year. Regressions were developed for all three analysis methods based on slab size for all 7 AMDAT zones, for a total of 21 regressions.

The statistical significance of each variable was tested and it was found that the only significant variables on the reference month HMA Modulus were the reference month mid-depth HMA temperature, the HMA thickness, and the project latitude, longitude, and elevation. The reference month mid-depth HMA temperature data was taken from the EICM data. The developed regression models are summarized below for both methods and all seven zones in Equation **Error! Reference source not found.**6) and Table 14.

$$E_{HMA(Ref)} = C_1 + C_2 * T_{Mid-Depth(Ref)} + C_3 * h_{HMA} + C_4 * Latitude + C_5 * Longitude + C_6 * Elevation \quad (16)$$

Where $E_{HMA(Ref)}$ is the reference month HMA Modulus, $T_{Mid-Depth(Ref)}$ is the reference month mid-depth HMA temperature, h_{HMA} is the HMA thickness (inches), and the Latitude, Longitude, and Elevation are for the project location

Table 14: Regression Coefficients for Reference Month HMA Modulus Equations

≤ 4.5 ft × 4.5 ft joint spacing	C1	C2	C3	C4	C5	C6	R^2
Zone 1	6902212	-58060.5	-36684	-48511	-3980.3	-9.91	0.901
Zone 2	5746174	-48590	-45205	-32771	505.3	-31.81	0.687
Zone 3	3919812	-20078.4	-45233	17658	-12374.7	52.25	0.654
Zone 4	3951615	-52629	-46317	25747	-2356	17.61	0.859
Zone 5	6172028	-62418	-69110	-31747	1793.9	4.801	0.908
Zone 6	5657489	-48939	-52613	-11091	-7769	-4.95	0.911

Zone 7	4050512	-39010	-56927	35689	-10707	88.486	0.856

> 4.5 ft and ≤ 7 ft joint spacing	C1	C2	C3	C4	C5	C6	R^2
Zone 1	516844	-35706	-65351	-22220	-6306	30.121	0.623
Zone 2	5396644	-40139	-89164	-32803	4454	-45.742	0.558
Zone 3	333077	-26639	-73246	30958	-7350	64.1	0.546
Zone 4	3458108	-35086	-31812	20508	-1956	47.1	0.590
Zone 5	3849527	-45022	-3932	2710	1245	48.4	0.723
Zone 6	3912042	-40680	-8978	-12689	3328	25.1	0.798
Zone 7	3901375	-44662	-10529	36735	-7709	15.89	0.824

> 7 ft longitudinal joint spacing	C1	C2	C3	C4	C5	C6	R^2
Zone 1	2491478	-10560	-142588	-11145	1813.8	-0.423	0.681
Zone 2	2076287	-6963	-146622	-198	596.9	4.914	0.711
Zone 3	2173722	-586.2	-145128	-4937	-381.7	3.028	0.706
Zone 4	2058023	-1519	-137632	99	-1295.7	5.391	0.685
Zone 5	2174744	-6379	-123582	-3127	69.6	-0.576	0.627
Zone 6	1718085	-2601	-107895	-3189	1959	-9.12	0.594
Zone 7	1734430	-7589	-112461	7729	1172	-2.32	0.687

High R^2 values for each regression indicate good predictability of the regression models, which can also be seen in **Error! Reference source not found.**4. This plot shows the variation between original reference month HMA Modulus and predicted reference month HMA Modulus using all of the regression models.

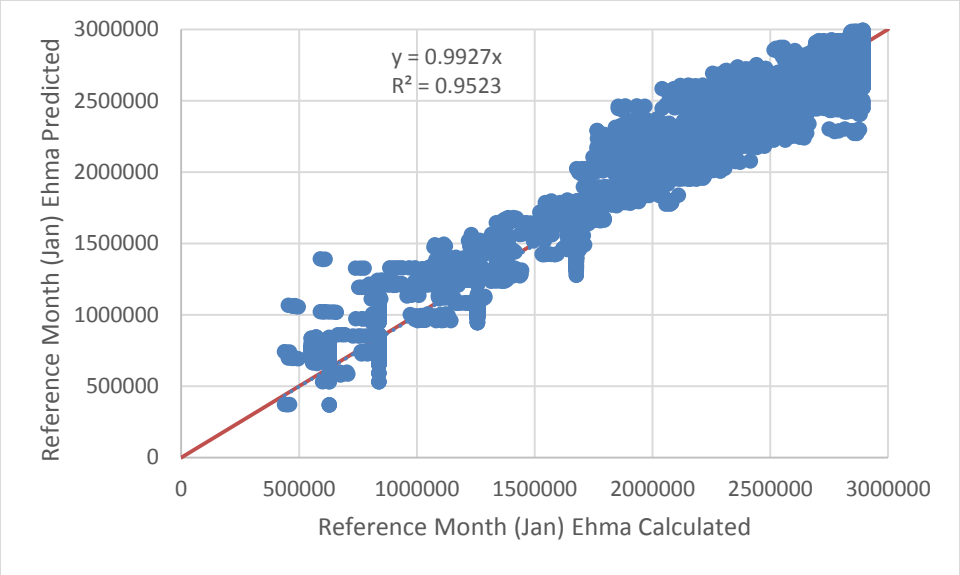

Figure 234: Predictability test of the $E_{HMA(Ref)}$ regression models.

Recommended reference month mid-depth HMA temperatures are provided for each month and AMDAT Zone in Table 15. These values were obtained based upon averages for every weather station used in the study.

Table 15: Recommended $T_{Mid-Depth(Ref)}$ for each AMDAT Zone

	Avg. Reference Month (Jan) Mid Depth HMA Temp (^{o}F)	Std. Dev. Reference Month (Jan) Mid Depth HMA Temp (^{o}F)
Zone 1	27.37	7.75
Zone 2	29.58	5.61
Zone 3	33.67	6.31
Zone 4	37.64	6.83
Zone 5	46.53	6.64
Zone 6	46.63	9.13
Zone 7	51.49	11.30

2.4. Procedure to Characterize the HMA Modulus

Step 1. Select the temperature zone for the whitetopping project based on its annual mean daily average temperature (AMDAT) or the location of the project site using Figure 3.

Step 2. Determine the F for each month for the selected zone using corresponding regression model from Equation **Error! Reference source not found.**) and coefficients from Table 12. Use the HMA thickness and normalized mid-depth HMA temperature.

Step3. Determine the reference month stiffness for the selected zone using the corresponding regression model from Equation (16) and the coefficients in Table 14. Use the HMA thickness, project latitude, project longitude, project elevation, and the reference month mid-depth HMA temperature.

Step 4. Determine the monthly HMA moduli by multiplying *F* for different months with HMA modulus for the reference month.

2.5. Summary of HMA Modulus Characterization

The change of HMA stiffness can be well predicted knowing its temperature, i.e. mid-depth HMA temperature. The analysis of the temperature data of the MnROAD and Elk River whitetopping cells indicated that the mid-depth HMA temperature is mainly a function of the ambient temperature. The ambient temperature varies with time and location. In order to establish the relation between HMA modulus and mid-depth temperature, the continental (lower 48) United States was divided into seven different zones according to the annual mean ambient temperature. For each zone, models for adjustment factors were developed for the HMA modulus to take into account the effect of temperature variation on the change of HMA modulus. Utilizing the developed adjustment factors for HMA modulus, designers can calculate the monthly HMA stiffness over the design life, in conjunction with the stiffness of the reference month determined from the appropriate regression models.

3. TEMPERATURE GRADIENT WITHIN THE PCC OVERLAY

The other primary effect that the climate has on the performance of UTWs and TWTs is the development of temperature gradients within the slab. The temperature gradient causes the slab to curl, resulting in additional stress, and consequently more fatigue damage in the overlay. Previously developed (or alternative) whitetopping design procedures consider the effect of temperature gradients by introducing a stress component in addition to the one due to traffic

loading. As mentioned in the introduction, however, little guidance has been provided on how to establish this temperature gradient for a specific UTW/TWT project.

In response to this need, one of the objectives in this task was to develop guidelines for establishing this input for the projects to be constructed throughout the United States. Two problems arose when addressing this objective. The first problem was derived from the fact that the temperature gradient is primarily a function of climatic conditions, and that for a geographic region as large as the United States, there is great variability in climate. This problem was overcome by establishing a relationship between the temperature gradients and the climate based on a database populated using the EICM. The other problem was an incompatibility in the temperature gradients required by the design guides, and the temperature gradients generated by the EICM. The temperature gradient input required by the alternative whitetopping design procedures is a single effective linear temperature gradient that remains constant throughout the design life (Mu and Vandenbossche, 2010). The EICM, however, provides the prediction of temperatures at designated depths which are nonlinear in nature and are provided on an hourly basis.

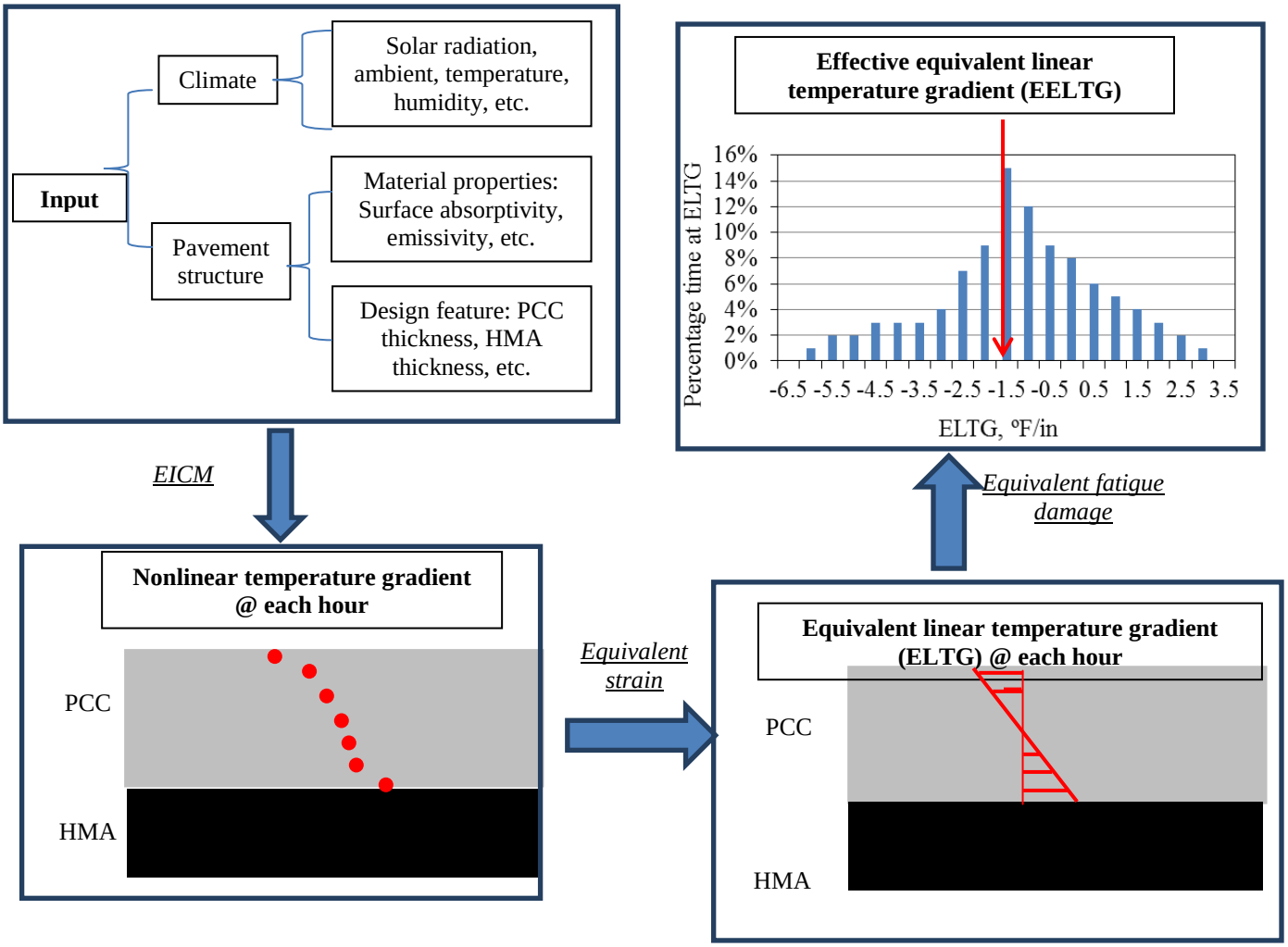

Figure 24: Procedure to generate the effective equivalent linear temperature gradient.

The framework used to solve the two problems and establish guidelines for establishing the input of temperature gradient is illustrated by

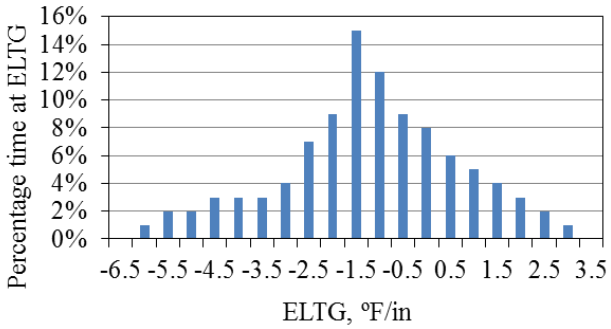

Figure 24. A database of hourly nonlinear temperature gradients was first populated through many EICM runs that included a large range of climatic conditions and whitetopping structures. The hourly nonlinear temperature gradients were then converted to hourly equivalent linear temperature gradients (ELTGs) based on the strain-equivalency principle used by Janssen and Snyder (2000). Finally, an effective equivalent linear temperature gradient (EELTG) was obtained. The EELTG is an equivalent linear temperature gradient that when applied throughout the design life results in the same fatigue damage as if the actual temperature gradients were used in an hourly analysis. The details of each step in

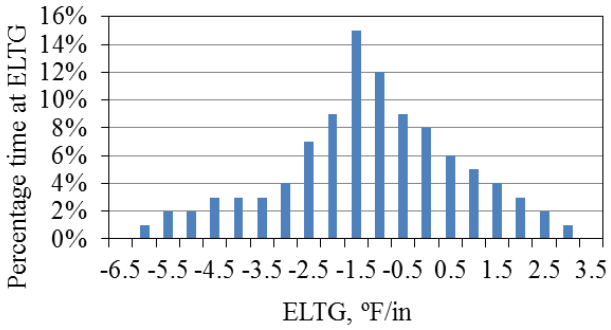

Figure 24 will be discussed in later sections.

3.1. Populating Database of Hourly Nonlinear Temperature Gradients for Various Climates and Pavement Structures

As mentioned previously, the extensive database required to produce a representative number of samples for analysis of all the climatic conditions in the United States was populated using the EICM. Specific weather stations were chosen to represent all the climatic conditions in the continental United States.

In total, 194 weather stations were selected, as shown in Table A1 in the Appendix. The selected stations are scattered widely and evenly as shown in Figure 25. The frequency of the elevations for the selected stations is summarized in Figure 26. It shows that the elevation of about 60% of the locations evenly distributes between 0 than 1500 ft and the elevation of other locations evenly distribute between 1500 ft and 7700 ft.

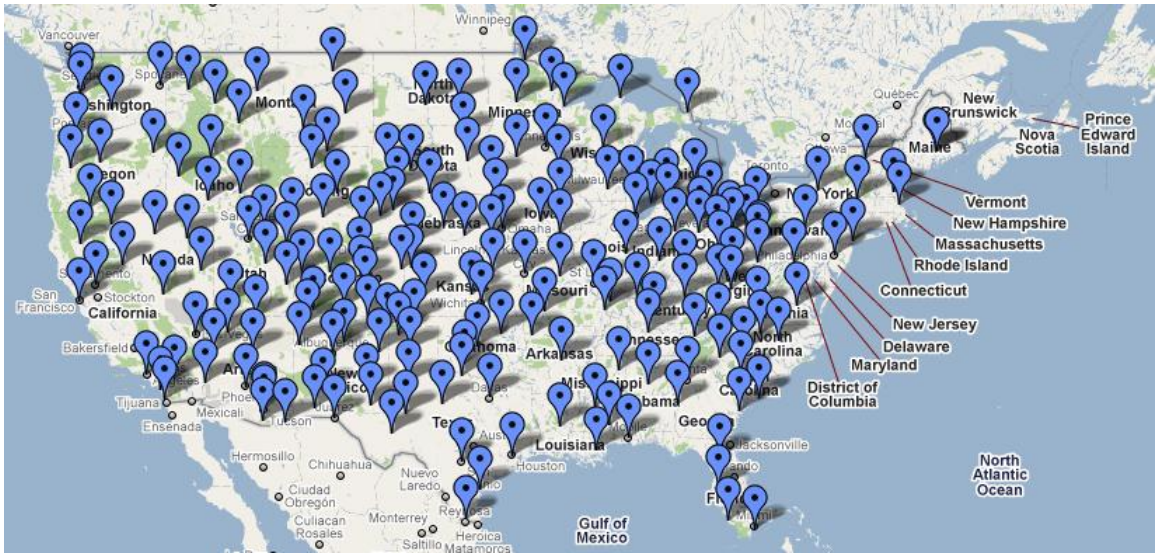

Figure 25: Locations of the Selected Weather Stations (The background map is the Google Map of the US as of June, 2010).

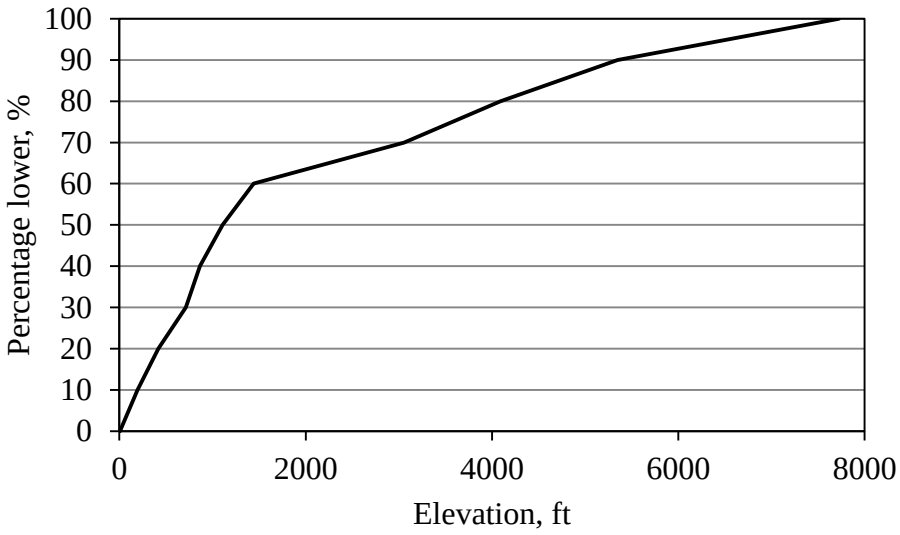

Figure 26: Frequency of Elevations of the Selected Weather Stations.

For each weather station, hourly climatic conditions over a one-year period were obtained for ambient temperature, wind speed, sunshine, precipitation, and relative humidity. This hourly climatic data, along with material property inputs, are required by the EICM to calculate the hourly temperature profiles to populate the required database. In addition to calculating the temperature profiles, statistical indicators such as the mean and standard deviation of the hourly climatic features were computed over the one-year period for each station, to aid in the

comparison of the results from the temperature gradient analysis. These statistics are presented in Table A2 in the Appendix.

Pavement features that were used in the EICM runs, and the fatigue analysis to be discussed in the following sections, are presented in **Error! Reference source not found.**. Considering the influence of pavement features on the fatigue analysis performed, a preliminary analysis indicated that the calculation of the EELTG using this approach is sensitive to slab size, asphalt thickness, concrete modulus of rupture and overlay thickness. The overlay thickness plays a particularly significant role in that it affects the temperature profiles generated by the EICM. This finding from the preliminary analysis agrees with the findings by Roesler et al. (2008). While the overlay thickness influences the ELTGs that are generated, the other three pavement features are indirectly significant through their influence on the fatigue analysis. In **Error! Reference source not found.**, the typical values selected for the overlay thickness and the slab size represent commonly used values for these parameters in current whitetopping practice. The after-milling asphalt thickness is assumed to be between 4 and 8-in based on the national survey carried out in Task 1 (Barman et al., 2010) of this project and the two values of concrete modulus of ruptures, i.e. 750 and 550 psi, represent strong and weak concrete, respectively. EELTG cases were calculated based on slab size: slabs with a joint spacing under 4.5 ft, slabs with a joint spacing between 4.5 ft and 7 ft, and slabs with a longitudinal joint spacing greater than 7 ft. An examination of all of the variables considered reveals that a total number of 24 EELTGs needed to be obtained for each weather station for slabs with a joint spacing less than 4.5 ft, while 18 EELTGs were required for the remaining two slab sizes. The parametric inferential space used in this study should be noted, so that caution can be observed when extrapolating results outside of this space.

In conducting the analysis to determine the EELTG for each station shown in Figure 25, the stiffness of the HMA layer used in the fatigue analysis was determined using the approach proposed in Section 2, namely the approach where the mid-depth HMA temperature was used with a site-dependent master curve to determine the HMA modulus. The Superpave binder grade typically used in the surrounding area of each weather station was obtained using the LTPPBIND version 3.1 software (Pavement System LLC, 2005), and the loading frequency of

10 Hz was used considering the effective length of the load pulse being approximately 60-in and a vehicle operational speed of around 35 mph. These values are believed to be typical for whitetopping applications.

3.2. Calculation of the Effective Equivalent Linear Temperature Gradient

3.2.1. Nonlinear Temperature Gradient

For each weather station, sixteen EICM runs were conducted for the typical whitetopping pavement structures defined in **Error! Reference source not found.**. As a result, temperatures were obtained at every inch throughout the depth of these pavements on an hourly basis.

3.2.2. Equivalent Linear Temperature Gradient

The nonlinear temperature profile for a specific hour generated by the EICM can then be converted into an equivalent linear temperature gradient (ELTG) based on Equations (17) to (19). This conversion was proposed by Janssen and Snyder (2000) to ensure that the resultant strains in the overlay under the ELTG and the nonlinear temperature gradient are the same.

$$T_{ave} = \sum_{i=1}^{n} \left[\frac{0.5(t_i + t_{i+1})(d_i - d_{i+1})}{(d_1 - d_n)} \right] \tag{17}$$

$$TM_0 = -0.25 \sum_{i=1}^{n} [(t_i + t_{i+1})(d_i^2 - d_{i+1}^2) - 2(d_1^2 - d_n^2)T_{ave}] \tag{18}$$

$$ELTG = -\frac{12 \cdot TM_0}{h^3} \tag{19}$$

where ELTG is the equivalent linear temperature gradient, °F/in; T_{ave} and TM_0 are the average temperature and temperature moment, respectively, °F·in^2; d_i is the depth of the *i*th node, inches; and t_i is the temperature at depth d_i, °F.

An equivalent linear temperature gradient obtained using Equations (17) through (19) will result in the same deflection profile of the slab as the actual nonlinear temperature profile. This is because a nonlinear temperature profile is the superposition of three components. These three components are the uniform temperature component, the equivalent-linear temperature

component and the nonlinear temperature component. The first component is responsible for uniform expansion and contraction of the slab while the second component results in curling of the slab. The last component, the non-linear portion of the temperature profile, results in no temperature moment and therefore does not influence the deflection profile of the slab when the second component is calculated based on the strain-equivalency principle. However, the third component will alter the internal stress distribution that is due to the first two components. Hiller and Roesler (2010) proposed an approach to estimate the stresses induced by the nonlinear component (the third component) of the actual temperature profiles assuming that the temperature profile can be represented by a quadratic function. The stress due to the equivalent linear temperature gradient obtained using Equations (17) through (19) can be adjusted using the approach to get the stress from the actual temperature profiles. They concluded that the critical stress at the top of the overlay is underpredicted when using only the equivalent linear temperature gradient. As part of this study, this procedure was applied to evaluate the prediction error of using only the equivalent linear temperature gradient at multiple locations across the country. Similar results were found among the locations that are in agreement with the conclusion by Hiller and Roesler (2010) and an example for Champaign, IL is presented in Figure 27. It shows that the stresses calculated using the strain-equivalent linear temperature gradient deviate about 5% from the stresses calculated based on the actual temperature profiles. This evaluation indicates the validity of using the strain-equivalent linear temperature gradient in predicting critical stresses for whitetopping.

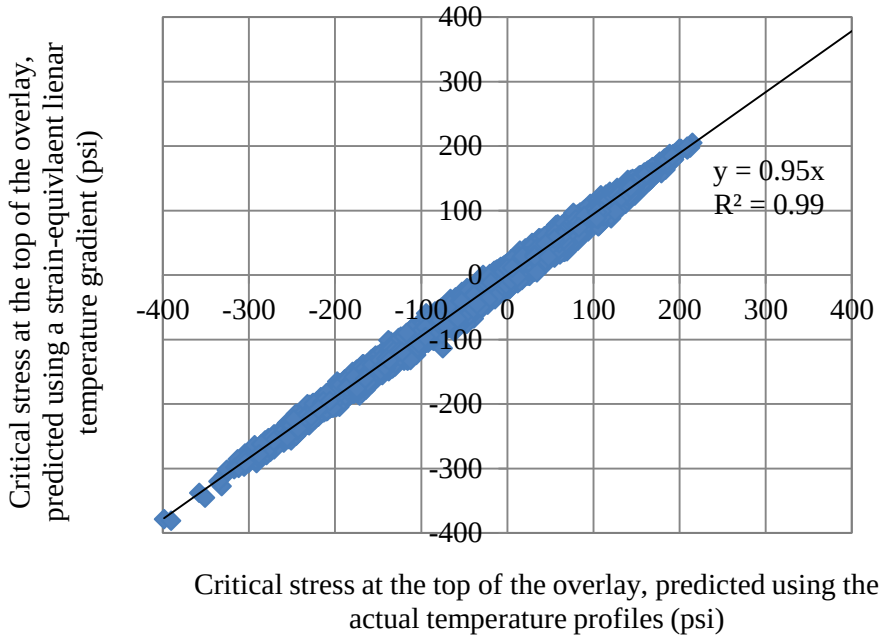

Figure 27: Comparison of the stresses using the strain-equivalent linear temperature gradient and the actual temperature profiles in predicting critical stresses, for 4-in overlay in Champaign, IL.

Another simpler way to obtain an ELTG based on a nonlinear temperature profile is to directly divide the difference in temperature between the top and the bottom of the overlay by the thickness of the overlay. This will be referred to as the direct-subtraction approach. While simpler, such an approach might introduce more significant errors for a highly nonlinear temperature profile then the strain-equivalency approach. A comparison between the two approaches was executed using the hourly ELTGs calculated with both methodologies and for each pavement section in the database of the previous section. As part of this analysis, it was found that the difference in the obtained ELTGs between the two approaches is mainly a function of the thickness of the overlay and is independent of the location. Two examples to illustrate this dependence are presented for the 4-in and 6-in overlays in Champaign, IL in Figure 28 and Figure 29, respectively. The absolute difference of the ELTGs between the approaches is relatively constant over the range of linear temperature gradients, namely about ±0.2 °F/in for the 6-in overlay and ±0.3 °F/in for the 4-in overlay. This implies that the error of using a direct-subtraction approach is more prominent for a thinner overlay.

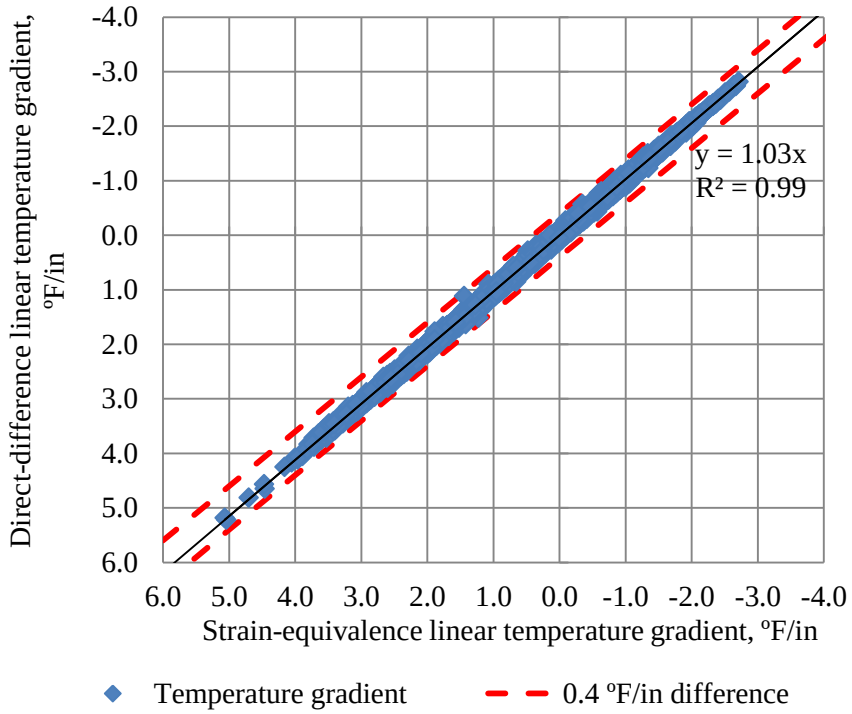

Figure 28: Comparison of the hourly ELTGs using the strain-equivalency approach and the direct-subtraction approach, for 6-in overlay in Champaign, IL.

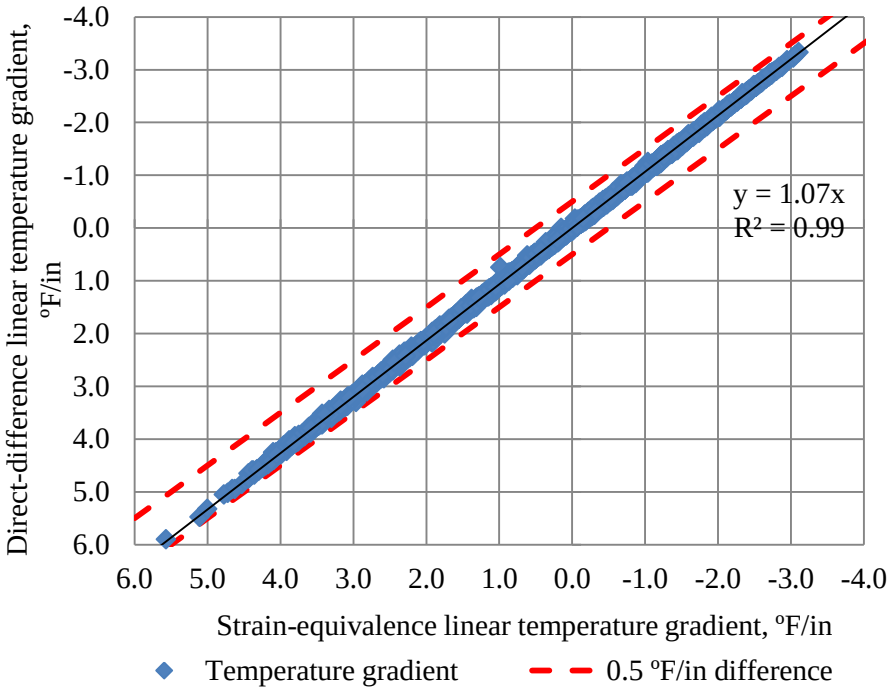

Figure 29: Comparison of the hourly ELTGs between using the strain-equivalency approach and the direct-subtraction approach, for a 4 in overlay in Champaign, IL.

3.2.3. Effective Equivalent Linear Temperature Gradient

Based on the calculated hourly ELTGs, one effective ELTG (EELTG) that results in the same fatigue damage as if the hourly ELTGs were applied was calculated. The ACPA fatigue model for PCC (Riley et al., 2005) was employed to carry out the fatigue analysis, where the allowable number of load repetitions, N_{PCC}, was determined as a function of the stress ratio, reliability level, and failure criterion in terms of cracking level, as shown in Equations (20) through (22).

$$\log N_{PCC} = \left[-\frac{SR^{-10.24}\log(R^*)}{0.0112} \right]^{0.217} \tag{20}$$

$$SR = \frac{\sigma_{TOTAL}}{M_R(1 + R_{150,3})} \tag{21}$$

$$R^* = 1 - \frac{(1 - R) \cdot P_{cr}}{0.5} \tag{22}$$

where N_{PCC} is the fatigue life in terms of the number of allowable repetitions; SR is the stress ratio; $\sigma_{TOTAL}$is the sum of the maximum stresses due to traffic and temperature difference in psi; M_R is the modulus rupture of the concrete in psi; $R_{150,3}$ is the residual strength ratio that characterizes the contribution of fiber reinforcement; R^* is the effective reliability at certain percentage of slabs cracked, P_{cr}. R^* would then be equal to R in Equation (22) when the failure is defined as 25 percent slabs cracked.

The total stress can be predicted using Equations (20) through (22). Only negative gradients were chosen in the analysis to be conservative. Considering only negative gradients is conservative, because negative (compressive) stress will be calculated if positive temperature gradients are used. This is a function of the fact that critical stresses at the top of the overlay are calculated, which is positive (tensile) only in the presence of negative gradients. The traffic parameters used in the fatigue analysis assumes that the trucks are evenly distributed among the twelve months and the hourly truck traffic distribution is as defined in Table 11.

3.3. Guidelines for Determining the Temperature Gradients

3.3.1. Correlation for the Prediction of EELTG

For each weather station in Table A1 of the Appendix, sixteen EELTGs were calculated for the combination of pavement structures presented in Table 10, using the nonlinear temperature gradients obtained from the EICM and the conversion, described in Section 3.2.

The location listed in Tables A1 and A2 contain whitetopping projects with various geographical, climatic and structural features, as well as the corresponding EELTGs for each individual project. The climate of each project is defined by the annual mean and standard deviation of the ambient temperature, wind speed, sunshine, precipitation and relative humidity. The pavement structural features include the overlay slab size, asphalt thickness, concrete modulus of rupture and overlay thickness.

Based on this database, a correlation can be established between the EELTGs and the geographical, climatic and pavement structure factors. Upon establishing this correlation, designers no longer need to use the EICM to estimate the EELTG directly, and can instead establish this value using a few project-specific inputs.

The variables considered in the regression analysis include the latitude, longitude, elevation, mean and standard deviation of annual ambient temperature, mean and standard deviation of annual wind speed, annual precipitation, mean and standard deviation of annual relative humidity, size of the PCC slabs, thickness of the asphalt layer, modulus of rupture of the PCC overlay and the thickness of the PCC overlay.

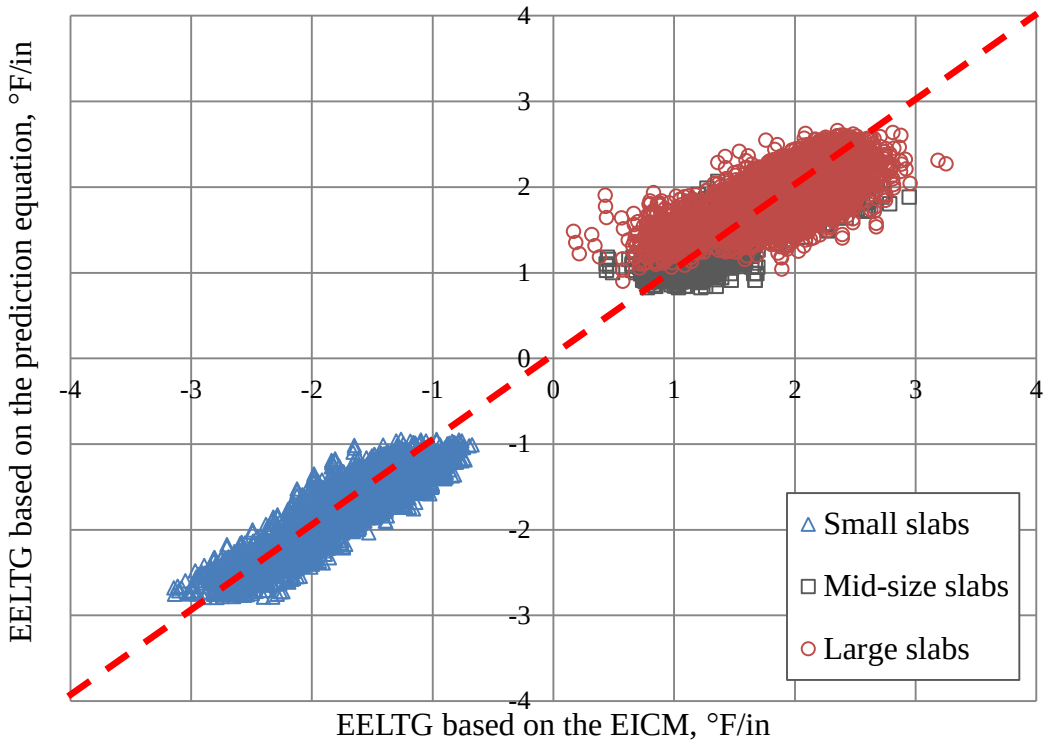

Figure 30: Variation in prediction of the EELTG using Equation for the pavement sections in the database used in this study.

A stepwise regression was performed to identify which variables are significant and which variables do not add accuracy to the equation proportional to the effort required to obtain these inputs for a given project. The small P-values (less than 0.0005) for all variables but the latitude imply that all the variables but the latitude are statistically sound in the regression. Based on regression analysis, Equation (23) is obtained using the coefficients found in Table 16. The correlation exhibits a good predictability of the EELTGs for the selected stations, as indicated by an adjusted R^2 values of 0.82, 0.59, and 0.48, depending on panel size. Figure 30 presents a summary of the deviation of the EELTG predicted using Equation (23) and Table 16 for each weather station from the values that were generated using the EICM. Smaller slabs, defined as those with a joint spacing less than or equal to 4.5 ft and larger slabs, defined as those with a joint spacing greater than 4.5 ft, have separate regression equations, and all coefficients are given in Table 16..

$$EELTG = C_0 + C_1 Latitude + C_2 Longitude + C_3 Elevation + C_4 S_{ave} + C_5 L - C_6 h_{HMA} + C_7 M_R + C_8 h_{pcc} \quad (23)$$

Table 16:: Coefficients for EELTG regressions based on slab size

	Joint spacing		
	≤ 4.5 ft	>4.5 ft and ≤ 7 ft	> 7 ft. longitudinal
C_0	0.534	0.85895	2.791
C_1	-0.0015677	0.0046918	0.011843
C_2	-0.0009853	0.0018581	0.0013466
C_3	-0.00002145	0.00000362	0.0000058
C_4	-0.0067836	0.0082567	0.009179
C_5	0.15843	0	0
C_6	-0.202627	-0.127695	-0.070225
C_7	-0.00175066	0.00077175	0.0013025
C_8	0	0	-0.45202
R^2	0.83	0.59	0.48

3.3.2. Inputs for the Correlation

In Equation (23), the pavement features are readily available and the annual mean temperature can either be obtained from local weather archives or easily determined based on the zonal division developed in Section 2. The difficulty in defining the inputs in Equation (23) lies in how to determine the annual mean percentage sunshine. The percentage sunshine is a variable defined in the EICM to characterize the solar radiation received. The intensity of the solar radiation is a function of the location (latitude, longitude and altitude), time (time of the day and day of the year) and the cloud coverage. In the EICM, the same relationship between the solar radiation and the time is applied everywhere, leaving the variation in solar radiation being a function of only the percentage of sunshine. Therefore, to practically solve this problem, the continental United States can be divided into zones based on the level of solar radiation. By dividing the continental United States into zones, typical values of the annual mean percent sunshine can be suggested for each zone. The map of annual concentrating solar resource was downloaded from the website of the National Renewable Energy Laboratory (NREL) (http://www.nrel.gov/gis/solar.html, as of May 2010), and as shown in Figure 31. Based on this map, the country can roughly be divided into six zones of solar radiation. For Zones 1 to 6, the number of weather stations is 30, 30, 30, 38, 32 and 34, respectively. The number of stations for each zone is fairly large making it possible to draw valid statistical conclusions on the average value of percent of sunshine for each zone.

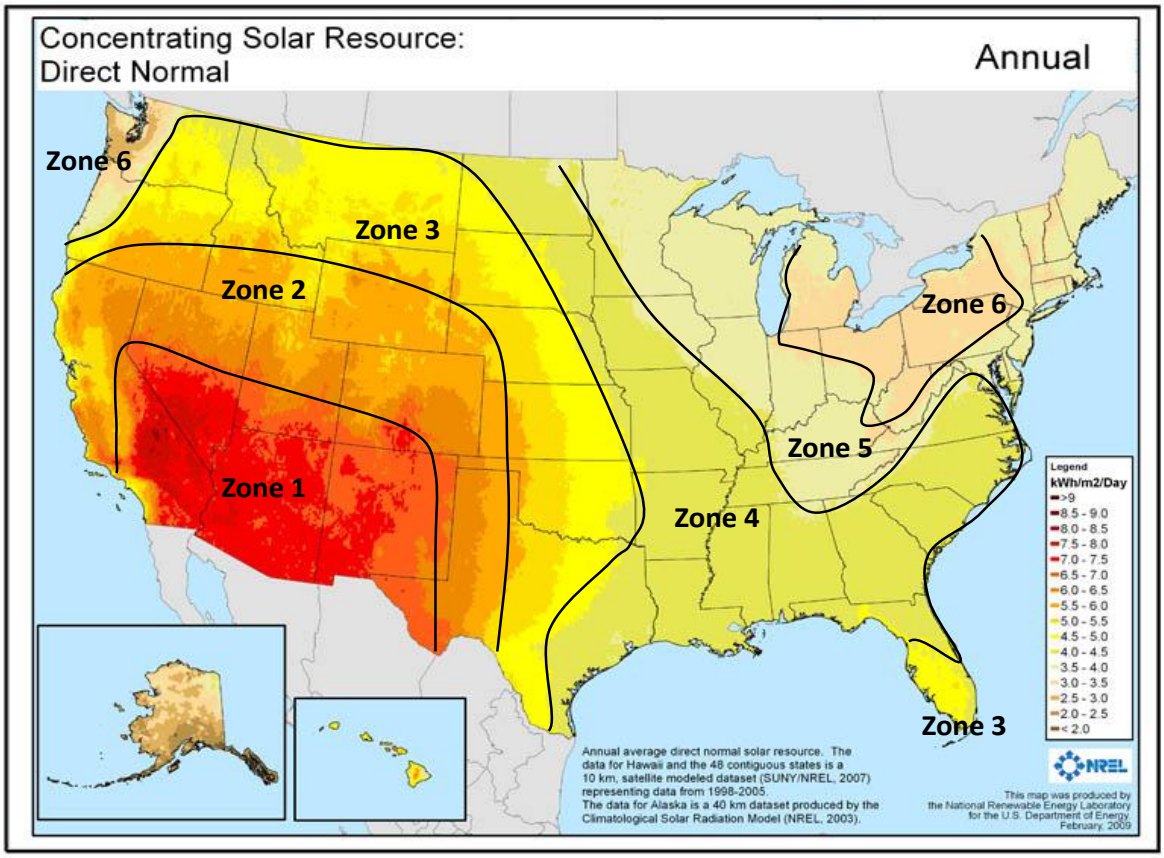

Figure 31: Annual concentrating solar resource map of the US in 2009 (http://www.nrel.gov/gis/solar.html, as in May 2010).

The frequency and magnitude of the percentage of sunshine for each zone is illustrated by the box plot as shown in Figure 32. It can be seen that zones with different solar radiation intensity sometimes exhibit similar annual mean percentages of sunshine. Therefore, typical values of annual mean percentages of sunshine can be suggested for new zones that are formed by combining Zones 1 and 2, Zones 3 and 4, and Zones 5 and 6, with a frequency distribution of the annual mean percentage of sunshine for the new zones illustrated by Figure 33, Figure 34 and Figure 35, respectively. The typical values of the annual mean percentage of sunshine were calculated and can be found in **Error! Reference source not found.**. The zonal average in Table 18 was then employed to predict the EELTG for each of the pavement sections in the database, and the results are presented in Figure 36. The use of the zonal averages results in an insignificant drop in the predictability of Equation (23) when compared with using the exact annual mean percentage of sunshine for each pavement section. Therefore, it might be

concluded that the zonal averages suggested in Table 18 can be used with confidence in Equation (23).

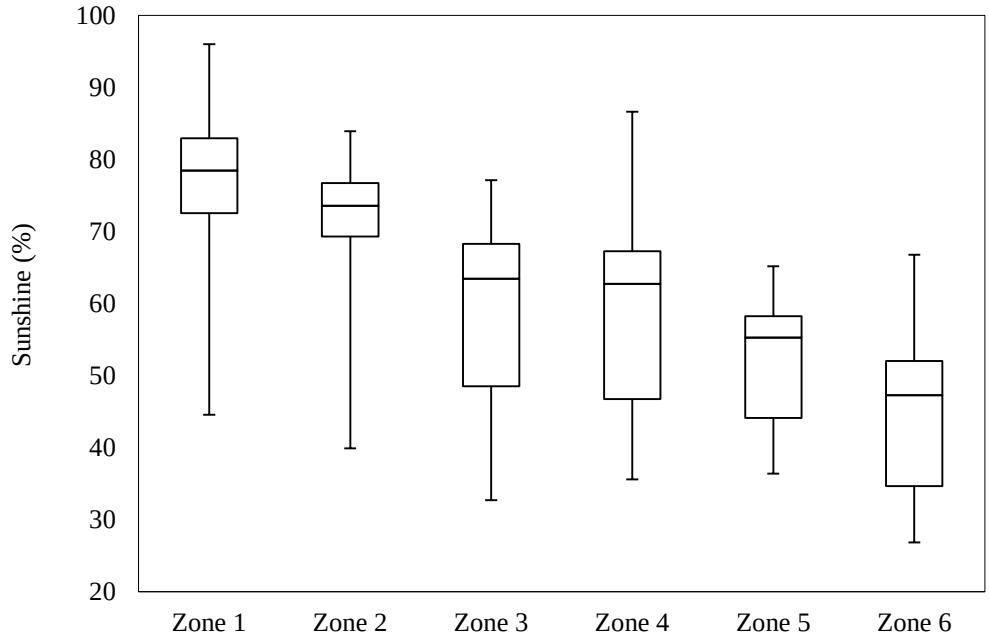

Figure 32: Statistics on the percentage of sunshine for the weather stations in each zone.

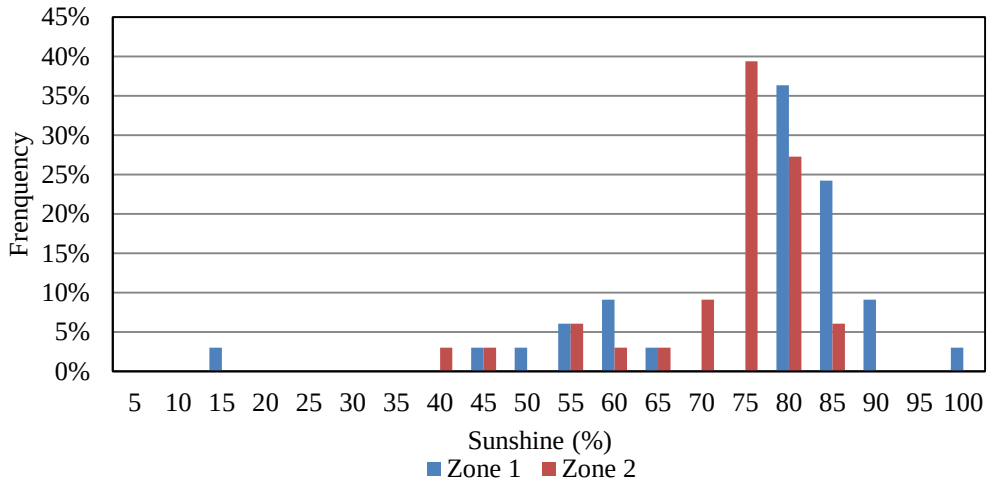

Figure 33: Frequency of the annual mean percentage of sunshine for Zones 1 and 2.

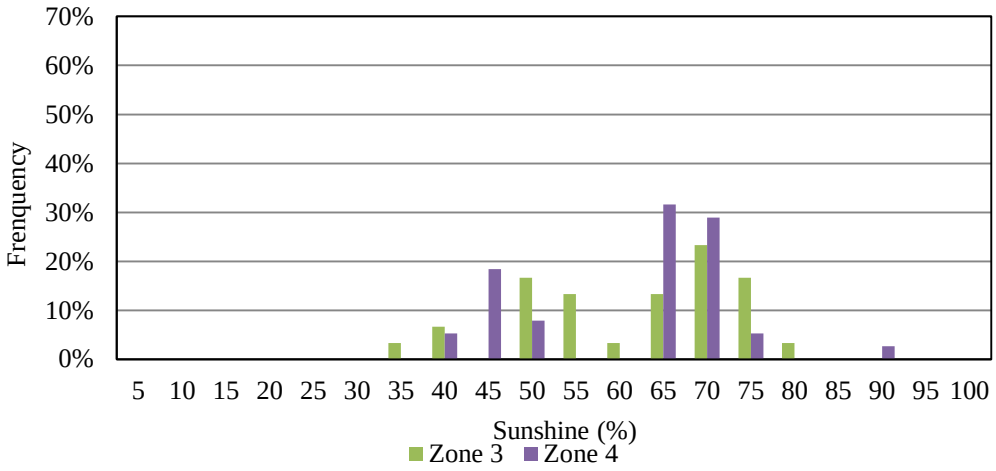

Figure 34: Frequency of the annual mean percentage of sunshine for Zones 3 and 4.

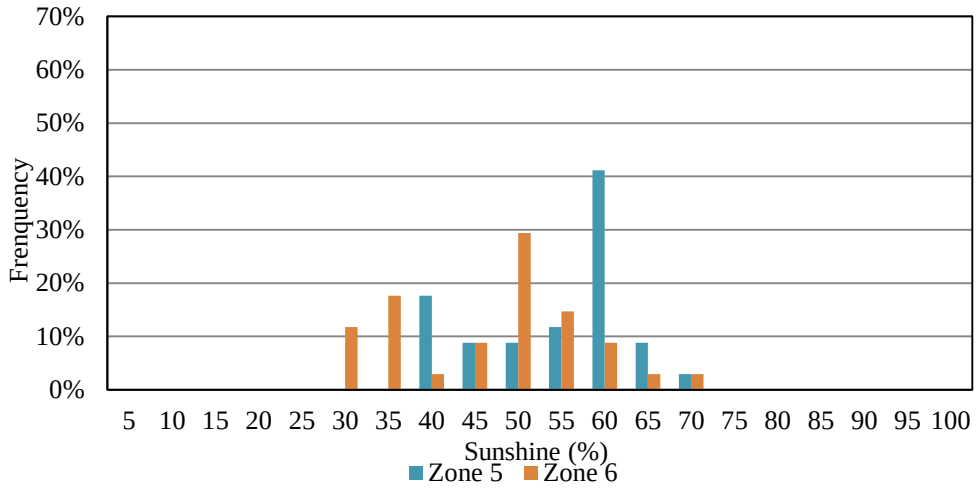

Figure 35: Frequency of the annual mean percentage of sunshine for Zones 5 and 6.

Table 17: Typical values for the annual mean percentage sunshine for each zone.

Zone	Mean (%)	Standard deviation (%)	Recommended zonal values (%)
1	73	17	90
2	71	10	80
3	59	12	60
4	59	12	50
5	52	9	40
6	44	11	30

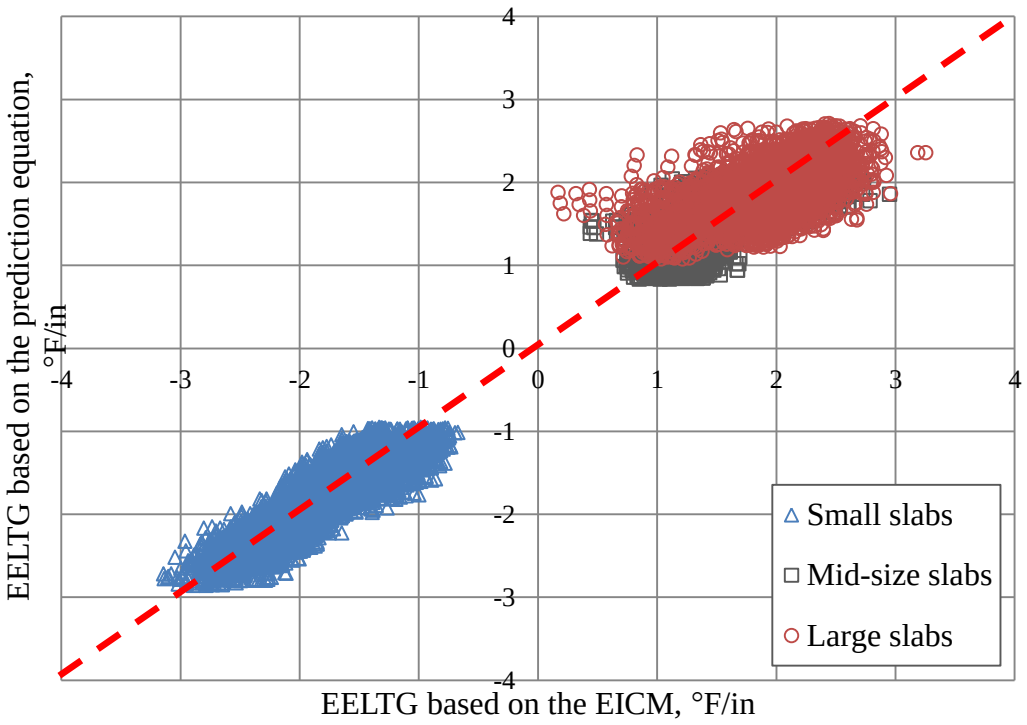

Figure 36: Variation in prediction of the EELTG using Equations **Error! Reference source not found.** and **Error! Reference source not found.** for the pavement sections in the database used in this study, using with the recommended zonal values for the percentage of sunshine.

3.4 Procedure to Calculate EELTG

Step 1. Determine the annual mean temperature based on the climatic file of the nearest weather station. The data from these weather stations is obtainable from the Transportation Research Board website: http://onlinepubs.trb.org/onlinepubs/archive/mepdg/climatic_state.htm. Another way to determine the annual mean temperature is to use the typical values provided in Figure 3 based on the project location.

Step 2. Calculate the annual mean percentage of sunshine based on the climatic file of the nearest weather station obtainable from the Transportation Research Board website: http://onlinepubs.trb.org/onlinepubs/archive/mepdg/climatic_state.htm. Another way to determine the annual mean percentage of sunshine is to use the typical values suggested in **Error! Reference source not found.** based on the climatic zones defined in Figure 31.

Step 3. Determine the EELTG using the climatic and geographical features as defined in Steps 1 and 2 and the pavement features in terms of the panel size, PCC overlay thickness, HMA layer thickness and the PCC modulus of rupture, based on Equation 23. The result is the EELTG that can be used in design.

3.5. Summary on PCC Temperature Gradient Characterization

In this section, the guideline to establish the EELTG that can be used in the whitetopping design procedures was developed. A number of weather stations (194 in total) were then selected within each climatic zone to be representative of all the possible combinations of climatic and geographical conditions. For each weather station, EICM runs were conducted for 16 predefined pavement structures. As a result, the hourly nonlinear temperature gradients were obtained for each pavement structure at each station. Based on strain equivalency, the hourly nonlinear temperature gradients were then converted to hourly ELTGs. These were then used to calculate the final product, the EELTG, based on fatigue analysis.

A stepwise linear regression was performed to develop a correlation between the EELTG and the annual mean ambient temperature, annual mean percentage of sunshine, PCC overlay panel size, overlay thickness, HMA layer thickness and the PCC modulus of rupture. To further facilitate designers in determining the annual mean percentage of sunshine, typical values were suggested for each of 6 climatic zones based on a statistical analysis of the annual mean percentage sunshine.

In addition to providing guidance on the determination of the annual mean percentage of sunshine, a step-by-step procedure on how to determine the EELTG for a particular project is also provided.

4. CONCLUSIONS

This report presented the findings of Task 4 of the FHWA Pooled fund study to develop a rational mechanistic-empirical based design guide for thin and ultrathin whitetopping. The first part of the report focuses on the characterization of the seasonal variation in the HMA modulus, while the second part focuses on establishing the PCC temperature gradient characterization.

The first part includes a detailed investigation into the factors that affect the mid-depth HMA layer temperature and hence the HMA layer modulus. It was found that the season and location of the project significantly affect the HMA modulus whereas; design features such as thickness of PCC and HMA have a negligible effect. In order to establish the relation between HMA modulus and mid-depth temperature, the continental (lower 48) United States was divided into seven different zones according to the annual mean ambient temperature. With the knowledge of the HMA modulus for any arbitrary month, guidance is provided to derive the moduli value for all other months using the proposed HMA modulus adjustment factors that account for seasonal variation of the HMA modulus, in addition to the effect of the hourly temperature variation on the fatigue of the overlay. In addition to providing guidance on how to establish the HMA modulus adjustment factors, regression models were developed for the reference month HMA modulus to avoid requiring the HMA modulus as an input.

In the second part of this report, a guide to predict the effective equivalent linear temperature gradient (EELTG) that is required by the structural model in the whitetopping design methods was developed in a rational, yet practical manner. The proposed equation for establishing the EELTG was established based on EICM runs using climatic database that represent the various climates across the country. This equation accounts for the climatic, geographical, and pavement features. In addition to being versatile across a wide range of climates, the equation developed to determine the EELTG is also readily applicable and requires only six easily defined inputs. These inputs are the annual mean temperature, annual mean percentage of sunshine, PCC overlay panel size, PCC overlay thickness, HMA layer thickness and the PCC modulus of rupture. Furthermore, an effort was made to suggest typical values for the annual mean percentage of sunshine. Typical values are defined for the six climatic zones.

REFERENCES

American Association of State Highway and Transportation Officials. (1993). AASHTO Guide for Design of Pavement Structures. Washington, DC.

ARA, I., ERES Consultants Division. (2004). Guide for Mechanistic-Empirical Design of New and Rehabilitated Pavement Structures. NCHRP Project 1-37A, Final Report. Transportation Research Board of the National Academies, Washington, DC.

ASTM D 2493. (1998). Viscosity-Temperature Chart for Asphalts. ASTM International, West Conshohocken, PA. Vol. 0.403, pp. 230-234.

ASTM D 4123-82. (1995). Standard Test Method for Indirect Tension Test for Resilient Modulus of Bituminous Mixtures. ASTM International, West Conshohocken, PA.

Barman, M., Vandenbossche, J. M. and Mu, F. (2010). Development of a Rational Mechanistic-Empirical Based Design Guide for Thin and Ultrathin Whitetopping, Task 1: Identify, Collect, Compile and Review Performance Data and Information. FHWA Pooled Fund study, TPF 5-165, pp 1-98.

Cylne, T. R., Li, X., Marasteanu, O. M., Skok, E. L. (2003). Dynamic and Resilient Modulus of Mn/DOT Asphalt mixtures. MN/RC – 2003-09. Minnesota Department of Transportation Office of Research Services, St. Paul, MN.

Gucunski, N. (1998). Development of a Design Guide for Ultra Thin Whitetopping (UTW). FHWA report 2001-018, New Jersey Department of Transportation, Trenton, NJ.

Hiller, J. E. and J. R. Roesler. (2010). Simplified Nonlinear Temperature Curling Analysis for Jointed Concrete Pavements. Journal of Transportation Engineering. Vol.136, No. 7, pp. 654–663.

Inge, E. H. J. and Y. R. Kim. (1995). Prediction of Effective Asphalt Layer Temperature. Transportation Research Record. Transportation Research Board, National Research Council, Washington, DC. Vol.1473, pp. 93–100.

Janssen, D.J. and M. B. Snyder. (2000). The Temperature-Moment Concept for Evaluating Pavement Temperature Data. Journal of Infrastructure Engineering. Vol.6, No.2, pp. 81-83.

Kim, Y. R., B. O. Hibbs and Y. C. Lee. (1995). Temperature Correction of Deflections and Backcalculated AC Moduli. Transportation Research Board, National Research Council, Washington, DC. Vol. 1473, pp. 55-62.

Long-Term Pavement Performance. (2009). DVD Version 7.0, US Department of Transportation, Federal Highway Administration, Washington, DC.

Loulizi, A., G. W. Flintsch, I. L. Al-Qadi and D. Mokarem. (2006). Comparing Resilient Modulus and Dynamic Modulus of Hot-Mix Asphalt as Material Properties for Flexible Pavement Design. Transportation Research Record, Transportation Research Board, National Research Council, Washington, DC, Vol.1970, pp. 161-170.

Pavement Systems LLC. (2005). LTTPBIND Version 3.1, A Superpave Binder selection Program, developed by Pavement Systems LLC for Federal Highway Administration Asphalt Team - HTA-23. Bethesda, MD.

Larson, G. and B. Dempsey. (2003). EICM Software. Enhanced Integrated Climatic Model Version 3.0 (EICM). University of Illinois, Urbana, IL.

Mu, F. and Vandenbossche, J. M. (2010). Development of a Rational Mechanistic-Empirical Based Design Guide for Thin and Ultrathin Whitetopping, Task 2: Evaluate Existing Performance Prediction/Damage Accumulation and Structural Response Models. FHWA Pooled Fund study, TPF 5-165, 2010, pp 1-147.

Riley, R. C., L. Titus-Glover, J. Mallela, S. Waalkes and M. Darter. (2005). Incorporation of Probabilistic Concepts into Fatigue Analysis of Ultrathin Whitetopping as Developed for the American Concrete Pavement Association. Proceedings from the Best Practices in Ultra Thin and Thin Whitetopping, Denver, CO, pp. 288-317.

Roesler, J., A. Bordelon, A. Ioannides, M. Beyer and D. Wang. (2008). Design and Concrete Material Requirement for Ultra-Thin Whitetopping. Research report FHWA-ICT-08-016. lllinois Center for Transportation, IL.

Sheehan, M., S. M. Tarr and S. Tayabji. Instrumentation and field testing of thin whitetopping in Colorado and revision of the existing Colorado thin whitetopping procedure. Report CDOT-DTD-R-2004-12. Colorado Department of Transportation, Denver, CO, 2004.

Tarr, S. M., M. Sheehan and P. A. Okamoto. (1998). Guidelines for the Thickness Design of Bonded Whitetopping Pavement in the State of Colorado. Report No. CDOT-DTD-R-98-10. Colorado Department of Transportation, Denver, CO.

Wu, C. L, S. M. Tarr, T. M. Refai, M. A. Nagi and M. J. Sheehan. (1999). Development of Ultra-Thin Whitetopping Design Procedure. PCA Research and Development, Serial No. 2124, Portland Cement Association, Skokie, IL.

Vandenbossche, J. M. (2001). The Measured Response of Ultra-Thin and Thin Whitetopping to Environmental Loads. 7th International Conference on Concrete Pavements, Orlando, Florida, USA, September, 2001.

Vandenbossche, J. M. and A. J. Fagerness. (2002). Performance, Analysis, and Repair of Ultrathin and Thin Whitetopping at Minnesota Road Research Facility. Transportation Research Record, Transportation Research Board, National Research Council, Washington, DC. Vol.1809, pp. 191–198.

APPENDIX

Table A1: Weather Stations for Each Climatic Zone.

Solar radiation zone number	AMDAT Zone	Location		Latitude (º)	Longitude (º)	Elevation (ft)
1	1	Douglas-Bisbee	AZ	31.28	109.36	4102
1	2	Flagstaff	AZ	35.08	-111.4	7003
1	2	Grand Canyon	AZ	35.57	-112.09	4292
1	5	Kingman	AZ	35.16	-113.56	4292
1	5	Nogales	AZ	31.25	-110.51	3887
1	4	Page	AZ	36.56	-111.27	4292
1	7	Phoenix	AZ	33.26	-111.59	1106
1	2	Window Rock	AZ	35.4	-109.04	821
1	7	Blythe	CA	33.37	-114.43	394
1	5	Los Angeles	CA	35.40	109.04	821
1	4	Oceanside	CA	33.13	-117.21	28
1	1	Alamosa	CO	37.26	-105.52	7536
1	2	Durango	CO	37.08	-107.46	6677
1	4	Albuquerque	NM	35.02	-106.37	5308
1	5	Carlsbad	NM	32.2	-104.16	821
1	5	Deming	NM	32.16	-107.43	4304
1	3	Farmington	NM	36.44	-108.14	5531
1	2	Gallup	NM	35.31	-108.47	4304
1	3	Raton	NM	36.44	-104.3	4304
1	5	Roswell	NM	33.19	-104.32	3652
1	3	Santa Fe	NM	35.37	-106.05	6335
1	4	Tucumcari	NM	35.11	-103.36	6335
1	2	Ely	NV	39.17	-114.51	6255
1	3	Reno	NV	39.29	-119.46	4407
1	3	Tonopah	NV	38.04	-117.05	2384
1	5	El Paso	TX	31.49	-106.23	3945
1	4	Guadalupe Pass	TX	31.05	-104.49	6677
1	3	Cedar City	UT	37.42	-113.06	5626
1	3	Moab	UT	38.46	-109.45	4575
1	7	Blythe	CA	33.37	114.43	394
1	7	Palm Springs	CA	33.50	116.31	447

Solar radiation zone number	AMDAT Zone	Location		Latitude (º)	Longitude (º)	Elevation (ft)
1	5	San Diego	CA	32.44	117.10	81
2	5	Alturas	CA	41.29	120.34	4090
2	5	Redding	CA	40.31	-122.19	513
2	4	Sacramento	CA	38.31	-121.29	41
2	6	San Francisco	CA	37.37	122.24	89
2	3	Burlington	CO	39.14	-102.17	4198
2	2	Colorado Springs	CO	38.49	-104.43	6183
2	2	Denver	CO	39.5	-104.4	5382
2	3	Grand Junction	CO	39.08	108.32	4826
2	3	Pueblo	CO	38.17	104.30	4655
2	3	Boise	ID	43.34	-116.13	2861
2	2	Pocatello	ID	42.55	-112.34	4454
2	2	Twin Falls	ID	42.29	-114.29	7143
2	3	Goodland	KS	39.22	-101.41	3657
2	3	Clayton	NM	36.27	-103.09	4971
2	1	Elko	NV	40.5	-115.47	7143
2	3	Winnemucca	NV	40.54	-117.49	6255
2	4	Guymon	OK	36.41	-101.31	3589
2	2	Klamath Falls	OR	42.09	-121.43	4090
2	4	Amarillo	TX	35.13	-101.43	3589
2	6	Fort Stockton	TX	30.55	-102.55	3015
2	5	Lubbock	TX	33.4	-101.49	3259
2	5	Midland	TX	31.56	-102.13	2866
2	2	Price	UT	39.33	-110.45	5877
2	3	Salt Lake City	UT	42.05	-111.58	4224
2	2	Vernal	UT	40.26	-109.31	5268
2	2	Casper	WY	42.54	-106.28	5351
2	2	Cheyenne	WY	41.1	-104.49	6128
2	1	Evanston	WY	41.16	-111.02	7143
2	1	Rawlins	WY	41.49	-107.12	4090
2	1	Rock Springs	WY	41.35	-109.04	821
3	7	Naples	FL	26.01	-81.47	21
3	7	Tampa	FL	27.58	-82.32	2271
3	1	Challis	ID	41.31	-114.13	5042
3	1	Mullan Pass	ID	47.28	-115.38	6074
3	4	Hutchinson	KS	38.04	-97.52	1523

Solar radiation zone number	AMDAT Zone	Location		Latitude (º)	Longitude (º)	Elevation (ft)
3	4	Manhattan	KS	39.08	-96.41	1045
3	5	Wichita	KS	37.39	-97.26	1341
3	2	Billings	MT	45.49	-108.32	3582
3	1	Butte	MT	45.58	-112.3	4292
3	1	Glasgow	MT	48.13	-106.37	2271
3	2	Great Falls	MT	47.28	-111.23	3673
3	1	Miles City	MT	46.26	-105.53	3945
3	1	Missoula	MT	46.55	-114.05	3202
3	5	Lawton	OK	34.34	-98.25	1110
3	4	Oklahoma City	OK	35.23	-97.36	1284
3	5	Tulsa	OK	36.12	-95.53	821
3	2	Redmond	OR	44.15	-121.09	3072
3	2	Philip	SD	44.03	-101.36	2208
3	2	Pine Ridge	SD	43.01	-102.31	3276
3	2	Rapid City	SD	44.03	-103.03	3153
3	5	Abilene	TX	32.25	-99.41	1792
3	5	Dallas	TX	32.54	-97.02	562
3	7	Mc Allen	TX	26.11	-98.14	4090
3	6	San Antonio	TX	29.32	-98.28	821
3	4	Wichita Falls	TX	33.59	-98.29	6183
3	2	Spokane	WA	47.37	-117.32	2384
3	2	Yakima	WA	46.34	-120.32	3652
3	1	Sheridan	WY	44.46	-106.59	3945
3	1	Worland	WY	43.58	-107.57	821
4	5	Birmingham	AL	33.34	-86.45	639
4	6	Mobile	AL	30.41	-88.15	212
4	4	Fayetteville	AR	36.01	-94.1	1247
4	5	Little Rock	AR	34.45	-92.14	292
4	6	Gainesville	FL	29.41	-82.16	152
4	5	Atlanta	GA	33.38	-84.26	974
4	5	Columbus	GA	32.31	-84.56	435
4	5	Savannah	GA	32.07	-81.12	51
4	3	Des Moines	IA	41.32	-93.4	971
4	2	Ottumwa	IA	41.07	-92.27	844
4	2	Sioux City	IA	42.23	-96.23	1139
4	5	Alexandria	LA	31.23	-92.18	97

Solar radiation zone number	AMDAT Zone	Location		Latitude (º)	Longitude (º)	Elevation (ft)
4	6	New Orleans	LA	29.59	-90.15	7
4	3	Hagerstown	MD	39.43	-77.44	737
4	4	Cape Girardeau	MO	37.14	-89.34	339
4	3	Columbia	MO	38.49	-92.13	884
4	3	Kansas City	MO	39.18	-94.43	1008
4	4	Springfield	MO	37.14	-93.23	1280
4	4	St Louis	MO	38.45	-90.22	710
4	5	Hattiesburg	MS	31.16	-89.15	147
4	5	Jackson	MS	32.19	-90.05	296
4	5	Tupelo	MS	34.16	-88.46	350
4	4	Charlotte	NC	35.13	-80.56	724
4	4	Greensboro	NC	36.06	-79.56	907
4	4	Raleigh/Durham	NC	35.52	-78.47	430
4	1	Bismarck	ND	46.46	-100.45	1654
4	1	Jamestown	ND	46.56	-98.41	1496
4	3	Lincoln	NE	40.5	-96.46	1204
4	3	Omaha	NE	41.19	-95.54	1028
4	5	Charleston	SC	32.54	-80.02	48
4	5	Columbia	SC	33.56	-81.07	365
4	4	Greenville	SC	34.51	-82.21	1037
4	1	Aberdeen	SD	45.27	-98.25	1306
4	1	Huron	SD	44.23	-98.14	1284
4	1	Sioux Falls	SD	43.35	-96.45	1428
4	6	Houston	TX	31.56	-95.22	121
4	5	Richmond	VA	37.31	-77.19	167
5	2	Waterloo	IA	42.33	-92.24	863
5	3	Carbondale/Murphyboro	IL	37.47	-89.15	430
5	3	Champaign	IL	40.02	-88.17	752
5	3	Chicago	IL	41.59	-87.55	658
5	4	Evansville	IN	38.02	-87.32	421
5	3	Indianapolis	IN	39.43	-86.16	797
5	4	Bowling Green	KY	36.59	-86.26	539
5	3	Lexington	KY	38.02	-84.37	980
5	3	Boston	MA	42.22	-71.01	180
5	3	Baltimore	MD	39.1	-76.41	196

Solar radiation zone number	AMDAT Zone	Location		Latitude (º)	Longitude (º)	Elevation (ft)
5	1	Bangor	ME	44.49	-68.49	197
5	2	Hancock	MI	47.1	-88.29	1073
5	1	Sault Ste Marie	MI	46.28	-84.22	727
5	1	Baudette	MN	48.44	-94.37	1083
5	1	Duluth	MN	46.5	-92.11	1429
5	1	Hibbing	MN	47.23	-92.5	1355
5	2	Minneapolis	MN	44.53	-93.14	874
5	1	Park Rapids	MN	46.54	-95.04	1453
5	1	Redwood Falls	MN	44.33	-95.05	1024
5	1	Rochester	MN	43.54	-92.29	1326
5	2	Manchester	NH	42.56	-71.26	269
5	2	Albany	NY	42.45	-73.48	281
5	3	New York	NY	40.4	-73.48	32
5	3	Cincinnati	OH	39.06	-84.25	512
5	4	Philadelphia	PA	39.52	-75.14	62
5	4	Knoxville	TN	35.49	-83.59	982
5	4	Nashville	TN	36.07	86.41	574
5	4	Roanoke	VA	37.19	-79.58	1192
5	2	Burlington	VT	44.28	-73.09	348
5	2	Madison	WI	43.08	-89.21	860
5	2	Milwaukee	WI	42.57	-87.54	680
5	2	Wausau	WI	44.56	-89.38	1192
6	2	Fort Wayne	IN	41.01	-85.13	806
6	2	Detroit	MI	42.13	-83.21	631
6	2	Grand Rapids	MI	42.53	-85.31	788
6	2	Kalamazoo	MI	42.14	-85.33	895
6	2	Saginaw	MI	43.32	-84.05	666
6	2	Binghamton	NY	42.13	-75.59	1630
6	1	Plattsburgh	NY	44.41	-73.31	352
6	2	Rochester	NY	43.07	-77.41	588
6	2	Syracuse	NY	43.07	-76.06	417
6	2	Watertown	NY	43.59	-76.01	332
6	3	Akron	OH	40.55	-81.26	1241
6	3	Cleveland	OH	41.24	-81.51	805
6	3	Findlay	OH	41.01	-83.4	800
6	2	Mansfield	OH	40.49	-82.31	1300

Solar radiation zone number	AMDAT Zone	Location		Latitude (º)	Longitude (º)	Elevation (ft)
6	3	Newark	OH	40.01	-82.28	882
6	3	Toledo	OH	41.34	-83.29	623
6	2	Youngstown/Warren	OH	41.15	-80.4	1193
6	3	Eugene	OR	44.08	-123.13	363
6	3	Portland	OR	45.35	-122.36	223
6	2	Altoona	PA	40.18	-78.19	1495
6	1	Bradford	PA	41.48	-78.38	2125
6	2	Du Bois	PA	41.11	-78.54	1807
6	2	Erie	PA	42.05	-80.11	756
6	3	Harrisburg	PA	40.11	-76.46	314
6	3	Pittsburgh	PA	40.3	-80.14	1175
6	2	Wilkes-Barre/Scranton	PA	41.2	-75.44	958
6	2	Williamsport	PA	41.14	-76.55	543
6	2	Bellingham	WA	48.47	-122.32	168
6	3	Seattle	WA	47.28	-122.19	450
6	3	Tacoma	WA	47.16	-122.35	296
6	3	Charleston	WV	38.23	-81.35	1026
6	3	Huntington	WV	38.23	-82.34	825
6	3	Morgantown	WV	39.98	-79.55	1245
6	3	Parkersburg	WV	32.92	-81.26	866

Table A2: Climatic Factors: Mean (M) and Standard Deviation (SD) for Each Selected Weather Stations.

Solar radiation zone number	AMDAT Zone	Location		Temperature (ºF)		Wind speed (mph)		Sunshine (%)		Annual precip (in)	Humidity (%)	
				M	SD	M	SD	M	SD		M	SD
1	1	Douglas Bisbee	AZ									
1	2	Flagstaff	AZ	47	19	5	5	76	38	20	55	26
1	2	Grand Canyon	AZ	50	19	5	4	81	30	14	48	22
1	5	Kingman	AZ	62	20	8	6	89	29	7	39	24
1	5	Nogales	AZ	62	17	5	4	87	30	20	47	25
1	4	Page	AZ	59	19	4	4	84	34	8	40	21
1	7	Phoenix	AZ	74	19	5	4	60	36	9	39	21
1	6	Tucson	AZ	69	18	6	4	82	28	13	43	23
1	2	Window Rock	AZ	48	20	5	5	78	36	11	56	27
1	7	Blythe	CA	74	19	6	5	96	17	3	34	19
1	4	Oceanside	CA	59	10	4	4	57	46	11	79	17
1	7	Palm Springs	CA	74	17	6	5	89	27	4	35	18
1	1	Alamosa	CO	42	22	6	5	80	36	11	56	24
1	2	Durango	CO	47	20	5	4	77	38	16	61	25
1	4	Albuquerque	NM	57	19	7	6	51	33	9	45	22
1	5	Carlsbad	NM	63	20	8	5	84	34	8	49	25
1	5	Deming	NM	61	19	7	5	82	27	9	44	23
1	3	Farmington	NM	53	20	7	4	78	37	108	51	25
1	2	Gallup	NM	49	21	6	5	78	37	12	54	26
1	3	Raton	NM	0	20	8	5	79	37	15	59	25
1	5	Roswell	NM	61	20	7	5	83	35	11	52	24
1	3	Santa Fe	NM	51	19	8	5	78	37	13	56	25
1	4	Tucumcari	NM	57	21	9	5	79	36	20	56	25
1	2	Ely	NV	46	21	8	4	76	39	7	52	27
1	6	Lasvegas	NV	69	20	7	5	63	35	5	33	19
1	3	Reno	NV	54	19	5	5	59	38	2	44	22

Solar radiation zone number	AMDAT Zone	Location		Temperature (ºF)		Wind speed (mph)		Sunshine (%)		Annual precip (in)	Humidity (%)	
				M	SD	M	SD	M	SD		M	SD
1	3	Tonopah	NV	51	20	8	5	85	32	5	44	22
1	5	El Paso	TX	65	18	7	5	54	33	6	40	20
1	4	Guadalupe Pass	TX	59	18	15	9	83	34	8	47	25
1	3	Cedar City	UT	50	21	5	5	76	38	13	49	24
1	3	Moab	UT	55	22	5	5	79	37	7	49	27
2	2	Alturas	CA	47	19	5	5	73	41	7	60	26
2	5	Redding	CA	62	18	5	5	74	39	29	56	26
2	4	Sacramento	CA	60	15	5	4	83	35	15	68	23
2	1	Aspen	CO	41	20	5	3	57	41	17	59	23
2	3	Burlington	CO	51	22	10	5	74	41	10	62	24
2	2	Colorado Springs	CO	48	20	8	5	65	36	14	56	25
2	2	Denver	CO	49	21	8	4	41	28	17	57	24
2	3	Boise	ID	51	20	6	4	71	42	9	59	25
2	2	Pocatello	ID	46	22	8	6	66	43	8	60	25
2	2	Twin Falls	ID	49	20	9	5	72	41	5	64	25
2	3	Garden City	KS	53	23	10	6	74	41	19	66	23
2	3	Goodland	KS	51	22	10	5	74	41	19	66	23
2	3	Clayton	NM	53	20	10	5	79	38	14	56	25
2	1	Elko	NV	45	24	4	4	71	42	7	54	26
2	3	Winnemucca	NV	50	21	6	4	78	38	6	54	26
2	4	Guymon	OK	56	22	9	5	77	39	17	59	24
2	2	Klamath Falls	OR	46	17	5	5	53	38	7	69	25
2	4	Amarillo	TX	57	21	11	5	76	40	20	61	25
2	3	Dalhart	TX	55	22	10	5	77	38	14	60	24
2	6	Fort Stockton	TX	67	18	10	4	84	34	180	50	24
2	5	Lubbock	TX	60	21	10	5	72	39	17	60	26
2	5	Midland	TX	64	20	9	5	79	38	11	56	25
2	2	Price	UT	49	20	6	4	77	38	8	52	23
2	3	Salt Lake City	UT	53	21	7	4	40	36	16	56	24
2	2	Vernal	UT	47	21	4	4	75	40	9	58	23
2	2	Casper	WY	45	23	10	6	75	40	7	58	24

Solar radiation zone number	AMDAT Zone	Location		Temperature (ºF)		Wind speed (mph)		Sunshine (%)		Annual precip (in)	Humidity (%)	
				M	SD	M	SD	M	SD		M	SD
2	2	Cheyenne	WY	46	20	10	6	69	42	16	58	23
2	1	Evanston	WY	42	20	8	5	69	42	9	59	25
2	1	Rawlins	WY	42	22	10	7	72	40	7	59	25
2	1	Rock Springs	WY	41	23	7	5	75	32	6	57	25
3	7	Miami	FL	76	8	7	4	40	28	61	74	13
3	7	Naples	FL	72	11	6	4	74	32	45	76	18
3	7	Tampa	FL	72	12	6	4	46	32	33	75	16
3	1	Challis	ID	42	23	4	4	68	43	5	57	24
3	1	Mullan Pass	ID	36	16	5	3	48	47	27	73	23
3	4	Hutchinson	KS	55	24	8	5	71	42	30	67	21
3	4	Manhattan	KS	54	24	7	5	71	42	33	69	20
3	5	Wichita	KS	57	23	10	5	45	38	27	66	21
3	2	Billings	MT	47	22	9	5	55	35	12	56	22
3	1	Butte	MT	38	22	5	4	61	45	12	64	23
3	1	Glasgow	MT	42	25	9	5	68	43	15	66	23
3	2	Great Falls	MT	45	22	10	6	54	40	11	57	23
3	1	Miles City	MT	45	25	8	5	68	43	16	65	23
3	1	Missoula	MT	43	20	4	4	53	46	15	68	22
3	5	Lawton	OK	62	21	8	5	73	41	29	67	22
3	4	Oklahoma City	OK	59	21	10	5	46	38	31	71	20
3	5	Tulsa	OK	61	22	8	5	51	38	30	69	20
3	2	Redmond	OR	47	18	5	4	65	44	6	65	25
3	2	Philip	SD	47	26	9	6	68	43	97	67	22
3	2	Pine Ridge	SD	47	24	7	5	67	44	18	65	22
3	2	Rapid City	SD	46	23	9	7	68	44	14	64	21
3	5	Abilene	TX	63	19	9	5	71	41	27	64	23
3	5	Dallas	TX	65	19	9	5	47	39	43	70	20
3	7	Mc Allen	TX	74	14	10	5	63	43	23	73	20
3	6	San Antonio	TX	68	16	7	4	36	37	41	73	21
3	4	Wichita Falls	TX	63	21	10	5	57	39	29	64	22
3	2	Spokane	WA	46	18	7	4	33	33	11	68	24
3	2	Yakima	WA	50	18	5	4	66	43	5	61	23
3	1	Sheridan	WY	44	24	6	6	64	42	9	63	22

Solar radiation zone number	AMDAT Zone	Location		Temperature (ºF)		Wind speed (mph)		Sunshine (%)		Annual precip (in)	Humidity (%)	
				M	SD	M	SD	M	SD		M	SD
3	1	Worland	WY	44	25	5	4	77	39	4	60	24
4	5	Birmingham	AL	62	17	5	4	43	38	62	72	20
4	6	Mobile	AL	66	15	6	4	69	41	64	76	20
4	4	Fayetteville	AR	56	20	5	5	67	43	43	75	20
4	5	Little Rock	AR	61	19	6	4	43	38	41	71	19
4	6	Gainesville	FL	67	14	5	4	69	40	44	75	21
4	5	Atlanta	GA	61	16	6	4	41	34	46	71	20
4	5	Columbus	GA	64	16	5	4	68	42	43	67	21
4	5	Savanah	GA	64	16	5	4	70	39	38	76	21
4	3	Des Moines	IA	49	24	9	5	42	41	25	72	17
4	2	Ottumwa	IA	49	24	9	5	62	44	41	76	16
4	2	Sioux City	IA	47	25	9	6	63	45	26	75	18
4	5	Alexandria	LA	64	17	4	4	64	43	58	81	20
4	6	New Orleans	LA	68	14	7	4	43	36	75	76	17
4	3	Hagerstown	MD	52	19	6	5	60	44	24	70	19
4	4	Cape Girardeau	MO	56	21	6	4	68	42	43	75	18
4	3	Columbia	MO	53	22	8	4	63	43	38	73	18
4	3	Kansas City	MO	53	23	9	4	44	38	51	73	17
4	4	Springfield	MO	55	21	7	4	66	44	42	72	18
4	4	St Louis	MO	56	22	8	4	40	38	30	69	18
4	5	Hattiesburg	MS	64	17	4	4	67	41	63	74	20
4	5	Jackson	MS	63	17	5	4	68	42	62	75	20
4	5	Tupelo	MS	60	19	5	4	68	42	60	71	19
4	4	Charlotte	NC	60	17	5	3	38	36	28	68	22
4	4	Greensboro	NC	57	17	6	4	46	39	38	68	21
4	4	Raleigh/Durham	NC	59	17	5	4	49	40	37	70	22
4	1	Bismarck	ND	43	26	8	5	62	44	25	73	18
4	1	Jamestown	ND	42	26	9	4	62	37	22	73	16
4	3	Lincoln	NE	51	24	9	5	63	42	28	70	18
4	3	Omaha	NE	50	24	9	5	61	43	29	73	17
4	5	Charleston	SC	64	16	7	4	73	39	46	74	20
4	5	Columbia	SC	63	17	5	4	48	40	35	68	22
4	4	Greenville	SC	61	16	6	4	67	43	37	67	21

Solar radiation zone number	AMDAT Zone	Location		Temperature (ºF)		Wind speed (mph)		Sunshine (%)		Annual precip (in)	Humidity (%)	
				M	SD	M	SD	M	SD		M	SD
4	1	Aberdeen	SD	42	27	9	6	64	45	25	76	17
4	1	Huron	SD	44	27	9	6	65	44	22	75	18
4	1	Sioux Falls	SD	44	26	9	6	62	45	28	75	18
4	7	Corpus Christi	TX	71	14	10	5	62	43	29	76	17
4	6	Houston	TX	67	16	6	4	36	34	64	78	19
4	5	Richmond	VA	62	17	5	4	87	30	20	47	25
5	2	Waterloo	IA	46	25	8	5	58	46	29	75	17
5	3	Carbondale/ Murphyboro	IL	55	21	6	5	64	44	41	75	18
5	3	Champaign	IL	51	22	9	5	59	42	30	76	19
5	3	Chicago	IL	49	22	8	4	39	37	32	71	18
5	4	Evansville	IN	55	20	6	4	65	43	41	73	18
5	3	Indianapolis	IN	52	21	8	4	36	38	38	72	17
5	4	Bowling Green	KY	57	20	5	4	62	44	39	72	18
5	3	Lexington	KY	55	20	6	4	59	44	38	72	19
5	3	Boston	MA	51	18	10	4	41	39	39	71	20
5	3	Baltimore	MD	55	18	6	4	41	36	39	68	21
5	1	Bangor	ME	44	21	7	5	57	45	23	72	20
5	2	Hancock	MI	41	21	9	5	46	47	24	79	16
5	1	Sault Ste Marie	MI	42	21	7	4	47	46	26	76	16
5	1	Baudette	MN	38	26	7	4	56	46	31	75	17
5	1	Duluth	MN	40	23	8	4	53	47	29	77	18
5	1	Hibbing	MN	38	24	6	4	55	46	25	78	18
5	2	Minneapolis	MN	45	25	8	4	37	37	34	70	18
5	1	Park Rapids	MN	40	26	8	5	55	47	23	74	18
5	1	Redwood Falls	MN	44	26	8	5	60	46	23	77	20
5	1	Rochester	MN	43	25	10	5	61	45	35	77	16
5	2	Manchester	NH	48	20	6	4	58	45	34	68	22
5	2	Albany	NY	48	20	6	5	60	44	31	72	19
5	3	Newyork	NY	53	17	10	5	40	35	37	70	20
5	3	Cincinnati	OH	54	19	5	4	56	45	42	75	19
5	4	Philadelphia	PA	55	18	8	4	43	38	39	67	20
5	3	Bristol/Jhns	TN	55	18	4	4	56	42	41	72	20

Solar radiation zone number	AMDAT Zone	Location		Temperature (ºF)		Wind speed (mph)		Sunshine (%)		Annual precip (in)	Humidity (%)	
				M	SD	M	SD	M	SD		M	SD
		n Cty/Kngsprt										
5	4	Knoxville	TN	58	18	5	4	54	40	42	71	19
5	4	Roanoke	VA	56	18	6	5	57	41	28	64	21
5	2	Burlington	VT	46	21	7	5	47	42	28	70	18
5	2	Madison	WI	47	23	6	4	55	44	33	73	17
5	2	Milwaukee	WI	47	21	9	4	40	37	38	73	16
5	2	Wausau	WI	45	23	7	4	54	46	28	75	18
6	2	Fort Wayne	IN	50	21	8	5	50	43	36	76	17
6	2	Detroit	MI	50	20	8	4	36	36	33	71	17
6	2	Grand Rapids	MI	48	20	8	4	31	33	34	76	16
6	2	Kalamazoo	MI	48	21	7	4	48	43	37	77	18
6	2	Saginaw	MI	48	20	8	4	33	37	24	76	17
6	2	Binghamton	NY	46	19	7	4	48	46	35	72	19
6	1	Plattsburgh	NY	44	22	5	4	48	44	27	71	19
6	2	Rochester	NY	48	19	8	5	30	34	30	74	17
6	2	Syracuse	NY	48	20	7	5	29	34	34	72	18
6	2	Watertown	NY	46	20	7	5	48	44	28	74	17
6	3	Akron	OH	49	20	7	4	28	32	32	76	18
6	3	Cleveland	OH	50	20	8	4	35	39	32	78	15
6	3	Findlay	OH	50	20	8	5	56	45	26	73	17
6	2	Mansfield	OH	49	20	8	4	53	46	29	76	17
6	3	Newark	OH	50	20	5	4	55	45	37	75	19
6	3	Toledo	OH	50	20	8	5	67	43	25	74	17
6	2	Youngstown /Warren	OH	49	20	7	4	29	33	29	74	18
6	3	Eugene	OR	51	13	5	4	53	46	21	79	19
6	3	Portland	OR	53	12	6	4	35	34	24	74	18
6	2	Altoona	PA	49	19	6	5	42	41	27	72	18
6	1	Bradford	PA	45	19	6	4	43	46	21	76	19
6	2	Du Bois	PA	46	20	7	4	46	46	34	73	20
6	2	Erie	PA	49	19	8	4	47	46	30	74	15
6	3	Harrisburg	PA	52	19	6	5	60	43	31	72	18
6	3	Pittsburgh	PA	50	19	6	4	30	34	35	72	19
6	2	Wilkes-	PA	49	19	6	4	57	45	28	69	19

Solar radiation zone number	AMDAT Zone	Location		Temperature (ºF)		Wind speed (mph)		Sunshine (%)		Annual precip (in)	Humidity (%)	
				M	SD	M	SD	M	SD		M	SD
		Barre/Scranton										
6	2	Williamsport	PA	50	19	5	4	48	43	34	71	20
6	2	Bellingham	WA	49	11	6	5	50	46	28	78	16
6	3	Seattle	WA	51	10	6	4	27	32	29	78	17
6	3	Tacoma	WA	51	10	5	4	46	43	33	78	17
6	3	Charleston	WV	54	19	3	4	48	39	42	75	21
6	3	Huntington	WV	54	19	5	3	57	45	39	75	20
6	3	Morgantown	WV	52	19	4	3	41	41	33	73	19
6	3	Parkersburg	WV	52	19	4	3	53	38	39	74	18